mathematics

MDPI

Article

A Novel Time Delay Nonsingular Fast Terminal Sliding Mode Control for Robot Manipulators with Input Saturation

Thanh Nguyen Truong, Anh Tuan Vo and Hee-Jun Kang *

Department of Electrical, Electronic and Computer Engineering, University of Ulsan, Ulsan 44610, Republic of Korea; truongthanhnguyen@mail.ulsan.ac.kr (T.N.T.); voanhtuan@mail.ulsan.ac.kr (A.T.V.)
* Correspondence: hjkang@ulsan.ac.kr; Tel.: +82-52-259-2207

Abstract: Manipulator systems are increasingly deployed across various industries to perform complex, repetitive, and hazardous tasks, necessitating high-precision control for optimal performance. However, the design of effective control algorithms is challenged by nonlinearities, uncertain dynamics, disturbances, and varying real-world conditions. To address these issues, this paper proposes an advanced orbit-tracking control approach for manipulators, leveraging advancements in Time-Delay Estimation (TDE) and Fixed-Time Sliding Mode Control techniques. The TDE approximates the robot's unknown dynamics and uncertainties, while a novel nonsingular fast terminal sliding mode (NFTSM) surface and novel fixed-time reaching control law (FTRCL) are introduced to ensure faster convergence within a fixed time and improved accuracy without a singularity issue. Additionally, an innovative auxiliary system is designed to address input saturation effects, ensuring that system states converge to zero within a fixed time even when saturation occurs. The Lyapunov-based theory is employed to prove the fixed-time convergence of the overall system. The effectiveness of the proposed controller is validated through simulations on a 3-DOF SAMSUNG FARA AT2 robot manipulator. Comparative analyses against NTSMC, NFTSMC, and GNTSMC methods demonstrate superior performance, characterized by faster convergence, reduced chattering, higher tracking accuracy, and a model-free design. These results underscore the potential of the proposed control strategy to significantly enhance the robustness, precision, and applicability of robotic systems in industrial environments.

Keywords: terminal sliding model control; robot manipulator; fixed-time control; time delay control; model-free control method; input saturation

MSC: 93B52; 93C10; 93C85

Academic Editor: Zhanybai T. Zhusubaliyev

Received: 1 December 2024
Revised: 26 December 2024
Accepted: 30 December 2024
Published: 31 December 2024

Citation: Truong, T.N.; Vo, A.T.; Kang, H.-J. A Novel Time Delay Nonsingular Fast Terminal Sliding Mode Control for Robot Manipulators with Input Saturation. *Mathematics* **2025**, *13*, 119. https://doi.org/10.3390/math13010119

1. Introduction

Manipulator systems are widely utilized in diverse fields, including industrial automation, daily tasks, and rescue missions, to handle complex, repetitive, and high-risk operations, thereby improving product quality, safety, and reliability. These applications require advancements in control strategies to achieve desired performance levels. As expectations for faster response times and enhanced precision increase, so does the need for more advanced control techniques. However, developing highly accurate controllers is a challenging task due to factors such as nonlinear behaviors, unpredictable disturbances, and dynamic environmental conditions.

Mathematical models of robotic system behavior are often developed using fundamental techniques, such as the Lagrange and Newton–Euler formulations or algorithms

like virtual decomposition. While these models effectively describe general dynamics, accurately identifying system parameters remains a significant challenge due to the unique designs of each robot, unknown uncertainties, and external disturbances. To overcome these difficulties and estimate manipulator dynamics, various soft computing techniques, such as fuzzy logic systems (FLSs) [1–3] and neural networks (NNs) [4,5], have been proposed. Although these methods effectively capture system behaviors, they often introduce challenges, including a large number of adjustable parameters, additional estimation errors, and high computational demands, which complicate real-time implementation.

TDE has recently emerged as a powerful and straightforward technique for approximating unknown dynamics in modern control systems [6,7]. The core concept of TDE is to use intentionally delayed measurements of acceleration and control input to estimate the current compensation term of the dynamics. TDE models system dynamics by dividing them into three distinct components: an acceleration term, which includes acceleration and its associated gain matrix; an offset term; and a control input term. By leveraging this unique mechanism, TDE eliminates the need for detailed knowledge of system dynamics, making it a simple yet effective model-free approach [8]. Its straightforward design and real-time implementation capabilities have led to its widespread adoption across various applications.

For instance, TDE has been successfully applied to approximate the complex dynamics of n-DOF manipulators, effectively addressing uncertainties [9]. In exoskeleton robots, TDE enables precise force control in virtual reality environments, even in the presence of dynamical uncertainties and bounded disturbances [10]. Furthermore, TDE achieves the desired tracking performance in the decoupling control of robotic systems [11].

The effectiveness of TDE has been extensively validated through rigorous theoretical analyses and experimental demonstrations, underscoring its practical significance. A robust and precise estimation mechanism, such as TDE, is essential for achieving optimal control performance in complex systems, including robotics. However, most TDE-based controllers employ linear error dynamics, which ensure only asymptotic stability [12,13]. This limitation prevents them from guaranteeing the rapid stabilization required for precise control within a fixed time frame. Additionally, the reliance on exact acceleration measurements presents a significant challenge in practical implementations.

Given these requirements, Sliding Mode Control (SMC) is often favored for its robustness to uncertainties, simplicity, and a wide range of applications [14]. However, analyses reveal that linear SMC methods only guarantee asymptotic error stability. To enhance convergence speed, sufficiently large reaching gains are required, particularly when the sliding mode surface approaches zero. To overcome this limitation, Terminal Sliding Mode Control (TSMC) techniques have been developed, introducing nonlinear functions into both the sliding surface design and the reaching control laws [15]. TSMC preserves the robustness of conventional SMC against uncertainties while ensuring finite-time convergence. In addition, super-twisting algorithms (STAs) have been introduced to achieve finite-time convergence, including the generalized super-twisting algorithm mentioned in [16]. However, STAs have certain limitations. For instance, they require knowledge of the bounds of disturbances and their derivatives for proper tuning. Additionally, parameter tuning is complex, and while chattering is reduced, it is not entirely eliminated. Residual chattering may still affect the performance of sensitive systems, particularly in high-precision applications.

The Terminal Sliding Mode (TSM) introduces a nonlinear sliding surface, often incorporating a negative exponential or fractional term in the tracking error, which enables finite-time convergence. However, as the tracking error approaches zero, the control input required by the TSM tends to infinity, resulting in singularity issues [15]. To address this

limitation, the Nonsingular Terminal Sliding Mode (NTSM) controller was developed, modifying the sliding surface design to eliminate the singularity problem and ensure smooth operation near zero tracking error, as discussed in [17,18].

As detailed in [17], an NTSM sliding surface is designed to ensure the finite-time convergence of the system trajectory when confined to this manifold. In addition, the studies [19,20] introduced fixed-time NTSMC that can ensure tracking error convergence in fixed time. To address mismatched disturbances, combinations of the NTSM with estimation methods or disturbance observers—such as FLSs [1,2], NNs [21–23], or high-order sliding mode observers [24,25]—have been developed, demonstrating excellent nominal performance recovery and reduced chattering effects. Furthermore, the fast stability, singularity-free behavior, and robust properties of the NTSM have been enhanced through the application of Nonsingular Fast Terminal Sliding Mode (NFTSM) controllers, which have been successfully implemented in robotic manipulators [26,27].

However, a significant challenge associated with various SMC techniques is the requirement for detailed knowledge of system dynamics. Additionally, to ensure stability and robustness, robust gains are typically chosen to exceed the upper bound of the lumped unknown terms, and these gains are combined with switching functions. However, this combination can induce chattering, resulting in high-frequency oscillations that may shorten the lifespan of system components [28].

To mitigate chattering, tuning laws for robust gains have been proposed, which rely on control error information. These laws activate the learning mechanism only after a sufficient amount of undesired control error has accumulated. While effective, this delay in activation may limit the adaptation speed of the learning mechanism. This underscores the need for further research to improve the efficiency of updating the robust gains or to explore alternative solutions that minimize the reliance on robust gains, thereby reducing chattering.

This challenge motivates the development of a controller that does not depend on the comprehensive dynamic information of the manipulator system. Such a controller, utilizing bounded smooth control inputs, must ensure fixed-time stability even in highly perturbed environments. This approach effectively addresses the challenges posed by system coupling, nonlinearity, and uncertainty, while significantly enhancing tracking performance.

In constrained control, input saturation—reflecting the capacity limitations of the plant—represents a significant source of performance degradation and can lead to instability, resulting in increased overshoot and tracking errors if not properly managed [29]. Several methods have been proposed to address control design under input saturation. For instance, a nonlinear saturated PID controller for robotic manipulators was introduced in [30], assuming knowledge of both the saturator and the system dynamics. The study [31] focused on global tracking and stabilization while accounting for external disturbances and input saturation. Additionally, learning control schemes for nonlinear uncertain systems with input saturation were explored in [32].

Adaptive neural network controllers have been utilized to address output constraints in uncertain systems [33], while adaptive tracking control for uncertain nonlinear systems with saturation was proposed in [34]. Furthermore, fuzzy controllers employing backstepping techniques for systems with unknown dead zones have also been discussed in [35]. Additional research has been conducted on neural network-based distributed adaptive approach and SMC [36].

Building on the previous discussions, this study presents an advanced orbit-tracking control strategy for manipulators. The main contributions of this research include the following:

- Effective approximation of the manipulator's dynamics using the TDE technique.

- Development of a novel SMC framework designed to achieve objectives such as a model-free design, high accuracy, robustness, reduced control input chattering, and faster convergence relative to contemporary fixed-time control methods. This approach is formulated based on equivalent control derived from TDE results, a new NFTSM surface, and a new FTRCL.
- Introduction of an innovative auxiliary system to address the effects of input saturation.
- Comprehensive proof of the fixed-time convergence and stability of the control system based on Lyapunov theory.
- Detailed analysis and validation of the proposed control strategy through simulations on a 3-DOF SAMSUNG FARA AT2 robot manipulator. The results demonstrate superior performance across various testing scenarios, with quantitative evaluations revealing improved tracking accuracy, faster convergence, reduced chattering, and enhanced robustness compared to NTSMC, NFTSMC, and GNTSMC methods.

The remainder of the paper is organized as follows: Section 2 provides the notations and preliminaries, Section 3 presents the detailed design of the proposed controller, Section 4 discusses the simulated validation in a robotic system, and Section 5 concludes the paper.

2. Notations and Preliminaries

2.1. Notations

The following notations are used consistently throughout this paper for clarity and convenience:

- For vectors $y = [y_1, y_2, \ldots, y_n]^T \in \mathbb{R}^n$ and $a = [a_1, a_2, \ldots, a_n]^T \in \mathbb{R}^n$:
  - $[y_1]^{a_1} = |y_1|^{a_1} \operatorname{sign}(y_1) \in \mathbb{R}$, where $\operatorname{sign}(y_1)$ denotes the sign function.
  - $y^a = [y_1^{a_1}, y_2^{a_2}, \ldots, y_n^{a_n}]^T \in \mathbb{R}^n$, with each component raised to its corresponding power.
  - $[y]^a = [[y_1]^{a_1}, [y_2]^{a_2}, \ldots, [y_n]^{a_n}]^T \in \mathbb{R}^n$, extending the operation component-wise with $[y_i]^{a_i} = |y_i|^{a_i} \operatorname{sign}(y_i)$.
  - $|y|^a = [|y_1|^{a_1}, |y_2|^{a_2}, \ldots, |y_n|^{a_n}]^T \in \mathbb{R}^n$, applying the absolute value to each component before raising it to the corresponding power.
- $\operatorname{diag}(y_1, \ldots, y_n) = \begin{bmatrix} y_1 & 0 & \ldots & 0 \\ 0 & y_2 & \ldots & 0 \\ \vdots & \vdots & \ddots & \vdots \\ 0 & 0 & \ldots & y_n \end{bmatrix} \in \mathbb{R}^{n \times n}$ is a diagonal matrix.
- The Euclidean norm is denoted as $\| \cdot \|$.

2.2. Preliminaries

Lemma 1. *Consider the system [27,37]:*

$$\dot{y} = -p_1 |y|^{j_1} - p_2 |y|^{j_2}, \tag{1}$$

where $p_1 > 0$, $p_2 > 0$, $j_1 > 1$, and $0 < j_2 < 1$. The origin of the system in (1) is fixed-time stable, with the settling time bounded by $T \leq T_{\max} = \frac{1}{p_1(j_1-1)} + \frac{1}{p_2(1-j_2)}$.

Lemma 2. *Consider the system [38]:*

$$\dot{y} = -d_1 |y|^{k_1} - d_2 |y|^{k_2}, \tag{2}$$

where $d_1 > 0$, $d_2 > 0$, and the exponents are defined as $k_1 = q_1^{sign(|y|-1)}$ and $k_2 = q_2^{sign(1-|y|)}$, with $q_1 > 1$ and $0.5 < q_2 < 1$. The origin of the system in (2) is fixed-time stable, and the settling time is bounded by:

$$\begin{aligned} T \le T_{\max} = & \min\left\{ \frac{1}{(q_1-1)d_2} \ln\left(1+\frac{d_2}{d_1}\right), \frac{q_2}{(1-q_2)d_1} \ln\left(1+\frac{d_1}{d_2}\right) \right\} \\ & + \min\left\{ \frac{1}{(1-q_2)d_1} \ln\left(1+\frac{d_1}{d_2}\right), \frac{q_1}{(q_1-1)d_2} \ln\left(1+\frac{d_2}{d_1}\right) \right\}. \end{aligned} \tag{3}$$

Lemma 3. *For any variable $y_i \in \mathbb{R}^+$, $i = 1, \ldots, n$, $\vartheta > 1$, $0 < \theta < 1$, the inequality always holds*

$$\sum_{i=1}^{n} y_i^{\vartheta} \ge n^{1-\vartheta} \left(\sum_{i=1}^{n} y_i\right)^{\vartheta}, \quad \sum_{i=1}^{n} y_i^{\theta} \ge \left(\sum_{i=1}^{n} y_i\right)^{\theta}. \tag{4}$$

3. Proposed Controller Design Process

3.1. Design of the Novel Fixed-Time Control System

Theorem 1. *Consider the following system:*

$$\dot{y} = -P^{-1}(y)(m_1[y]^{n_1} + m_2[y]^{n_2}) \tag{5}$$

where $P(y) = a + (1-a)/(1+r|y|^h)$, $0 < a < 1$, $r > 0$, h is an even positive integer, $m_1 > 0$, $m_2 > 0$, $n_1 = l_1^{sign(|y|-1)}$, $l_1 > 1$, $n_2 = l_2^{sign(1-|y|)}$, and $0.5 < l_2 < 1$.

The system in Equation (5) achieves fixed-time stability, and the maximum settling time is given by:

$$\begin{aligned} T_{max} = & \min\left\{ \frac{\bar{a}}{(l_1-1)m_2} \ln\left(1+\frac{m_2}{m_1}\right), \frac{l_2\bar{a}}{(1-l_2)m_1} \ln\left(1+\frac{m_1}{m_2}\right) \right\} \\ & + \min\left\{ \frac{1}{(1-l_2)m_1} \ln\left(1+\frac{m_1}{m_2}\right), \frac{l_1}{(l_1-1)m_2} \ln\left(1+\frac{m_2}{m_1}\right) \right\}, \end{aligned} \tag{6}$$

where $\bar{a} = a + \frac{1-a}{1+r}$.

Proof of Theorem 1. The proof considers two distinct cases: $|y| > 1$ and $|y| \le 1$.

Case $|y| > 1$: For this case, $n_1 = l_1 > 1$ and $n_2 = 1/l_2 > 1$. Thus, Equation (5) simplifies to:

$$\dot{y} = -P^{-1}(y)\left(m_1|y|^{l_1} + m_2|y|^{\frac{1}{l_2}}\right). \tag{7}$$

Let $\phi_1 = |y|^{1-l_1}$. Substituting this into Equation (7), we obtain:

$$\begin{aligned} \dot{\phi}_1 &= (1-l_1)|y|^{-l_1}\text{sign}(y)\left[-P^{-1}(y)\left(m_1|y|^{l_1} + m_2|y|^{\frac{1}{l_2}}\right)\right] \\ &= (l_1-1)P^{-1}(y)\left(m_1 + m_2\phi_1^{v_1}\right), \end{aligned} \tag{8}$$

where $v_1 = 1 - \frac{1-l_2}{l_2(l_1-1)} < 1$.

Note that $\lim_{|y|\to+\infty}\phi_1 = 0$ for $|y| \in [1, +\infty]$ and $\phi_1 \in (0, 1]$. Solving Equation (8), the convergence time is given by:

$$\begin{aligned}\int_0^{T_{s11}} dt &= \int_0^1 \frac{P(y)d\phi_1}{(l_1-1)\left(m_1+m_2\phi_1^{v_1}\right)}\\ T_{s11} &= \frac{1}{l_1-1}\int_0^1 \frac{P(y)d\phi_1}{m_1+m_2\phi_1^{v_1}}\\ &< \frac{1}{l_1-1}\int_0^1 \frac{P(y)d\phi_1}{m_1+m_2\phi_1}.\end{aligned} \tag{9}$$

Since $r > 0$ and h is an even positive integer, we have $r|y|^h \geq r$. Hence, $P(y) \leq \bar{a} < 1$, and Equation (9) simplifies further:

$$\begin{aligned}T_{s11} &< \frac{1}{l_1-1}\int_0^1 \frac{\bar{a}d\phi_1}{m_1+m_2\phi_1}\\ &< \frac{\bar{a}}{(l_1-1)m_2}\ln\left(1+\frac{m_2}{m_1}\right).\end{aligned} \tag{10}$$

Next, define $\beta_1 = |y|^{1-\frac{1}{l_2}}$. Substituting into Equation (7), the transformed system is:

$$\begin{aligned}\dot{\beta}_1 &= \left(1-\frac{1}{l_2}\right)|y|^{-\frac{1}{l_2}}\operatorname{sign}(y)\left[-P^{-1}(y)\left(m_1|y|^{l_1}+m_2|y|^{\frac{1}{l_2}}\right)\right]\\ &= \left(\frac{1}{l_2}-1\right)P^{-1}(y)\left(m_1\beta_1^{b_1}+m_2\right),\end{aligned} \tag{11}$$

where $b_1 = 1 - \frac{l_2(1-l_2)}{1-l_2} < 1$.

Similarly, $\lim_{|y|\to+\infty}\beta_1 = 0$ for $|y| \in [1, +\infty]$ and $\beta_1 \in (0, 1]$. Solving Equation (11), the convergence time is given by:

$$\begin{aligned}\int_0^{T_{s12}} dt &= \int_0^1 \frac{P(y)d\beta_1}{\left(\frac{1}{l_2}-1\right)\left(m_1\beta_1^{b_1}+m_2\right)}\\ T_{s12} &= \frac{l_2}{1-l_2}\int_0^1 \frac{P(y)d\beta_1}{m_1\beta_1^{b_1}+m_2}\\ &< \frac{l_2}{1-l_2}\int_0^1 \frac{\bar{a}d\beta_1}{m_1\beta_1+m_2}\\ &< \frac{l_2\bar{a}}{(1-l_2)m_1}\ln\left(1+\frac{m_1}{m_2}\right).\end{aligned} \tag{12}$$

From Equations (10) and (12), the settling time for $|y| > 1$ is:

$$T_{s1} = \min\left\{\frac{\bar{a}}{(l_1-1)m_2}\ln\left(1+\frac{m_2}{m_1}\right), \frac{l_2\bar{a}}{(1-l_2)m_1}\ln\left(1+\frac{m_1}{m_2}\right)\right\}. \tag{13}$$

Since $0 < \bar{a} < 1$, the convergence time of the proposed method is shorter than that described in Lemma 2.

Case $|y| \leq 1$**:** For this case, we have $n_1 = \frac{1}{l_1} < 1$ and $n_2 = l_2 < 1$. Therefore, Equation (5) reduces to:

$$\dot{y} = -P^{-1}(y)\left(m_1[y]^{\frac{1}{l_1}}+m_2[y]^{l_2}\right). \tag{14}$$

Let us define the variable $\phi_2 = |y|^{1-l_2}$. Then, $\phi_2 \in [0,\ 1]$ for $|y| \in [0,\ 1]$. Using this substitution, Equation (14) becomes:

$$\dot{\phi}_2 = -(1-l_2)P^{-1}(y)\left(m_1\phi_2^{v_2} + m_2\right), \tag{15}$$

where $v_2 = 1 - \frac{l_1-1}{l_1(1-l_2)} < 1$.

The convergence time can be derived by integrating Equation (15) as follows:

$$\begin{aligned} \int_0^{T_{s21}} dt &= \int_1^0 -\frac{P(y)d\phi_2}{(1-l_2)\left(m_1\phi_2^{v_2} + m_2\right)} \\ T_{s21} &= \frac{1}{1-l_2}\int_0^1 \frac{P(y)d\phi_2}{m_1\phi_2^{v_2} + m_2}. \end{aligned} \tag{16}$$

The convergence time for the method described in Lemma 2, denoted as T_{s21}^{LM2}, is:

$$T_{s21}^{LM2} = \frac{1}{1-l_2}\int_0^1 \frac{d\phi_2}{m_1\phi_2^{v_2} + m_2}. \tag{17}$$

Given $\bar{a} \leq P(y) < 1$ for $|y| \in (0,\ 1]$, it follows that $T_{s21} < T_{s21}^{LM2}$, and T_{s21} is bounded by:

$$\begin{aligned} T_{s21} &< \frac{1}{1-l_2}\int_0^1 \frac{d\phi_2}{m_1\phi_2 + m_2} \\ &< \frac{1}{(1-l_2)m_1}\ln\left(1 + \frac{m_1}{m_2}\right). \end{aligned} \tag{18}$$

Next, define $\beta_2 = |y|^{1-\frac{1}{l_1}}$, such that $\beta_2 \in [0,\ 1]$ for $|y| \in [0,\ 1]$. Substituting this variable, Equation (14) transforms into:

$$\dot{\beta}_2 = -\frac{(l_1-1)}{l_1}P^{-1}(y)\left(m_1 + m_2\beta_2^{b_2}\right), \tag{19}$$

where $b_2 = 1 - \frac{l_1(1-l_2)}{l_1-1} < 1$.

The convergence time for this case can be derived as:

$$\begin{aligned} \int_0^{T_{s22}} dt &= \int_1^0 -\frac{l_1P(y)d\beta_2}{(l_1-1)\left(m_1 + m_2\beta_2^{b_2}\right)} \\ T_{s22} &= \frac{l_1}{l_1-1}\int_0^1 \frac{P(y)d\beta_2}{m_1 + m_2\beta_2^{b_2}}. \end{aligned} \tag{20}$$

The convergence time of Lemma 2 in this case is:

$$T_{s22}^{LM2} = \frac{l_1}{l_1-1}\int_0^1 \frac{d\beta_2}{m_1 + m_2\beta_2^{b_2}}. \tag{21}$$

Since $\bar{a} \leq P(y) < 1$ for $|y| \in (0,\ 1]$, it follows that $T_{s22} < T_{s22}^{LM2}$, and T_{s22} is bounded by:

$$\begin{aligned} T_{s22} &< \frac{l_1}{l_1-1}\int_0^1 \frac{d\beta_2}{m_1 + m_2\beta_2} \\ &< \frac{l_1}{(l_1-1)m_2}\ln\left(1 + \frac{m_2}{m_1}\right). \end{aligned} \tag{22}$$

From Equations (18) and (22), the total settling time for $|y| \leq 1$ is given by:

$$T_{s2} = \min\left\{ \frac{1}{(1-l_2)m_1} \ln\left(1+\frac{m_1}{m_2}\right), \frac{l_1}{(l_1-1)m_2} \ln\left(1+\frac{m_2}{m_1}\right) \right\}. \tag{23}$$

Combining the results for $|y| > 1$ and $|y| \leq 1$, the overall settling time of the system described by Equation (5) is:

$$T_s = T_{s1} + T_{s2}. \tag{24}$$

The proof is now complete. □

Remark 1. *Based on the analysis above, it is evident that the proposed method achieves a faster convergence speed than the existing fixed-time control methods [27,37–39]. To validate this claim, numerical simulations were conducted to compare the convergence speed of the proposed method (MT3) with the methods described in Lemma 1 (denoted as MT1) and Lemma 2 (denoted as MT2). All control parameters for the methods were set identically, with values of* $p_1 = d_1 = m_1 = 2$, $p_2 = d_2 = m_2 = 2$, $j_1 = q_1 = l_1 = 1.5$, $j_2 = q_2 = l_2 = 0.7$, $a = 0.2$, $r = 20$, *and* $h = 2$. *Based on these parameters, the theoretical convergence times were computed as follows:* $T_{MT1} = 2.67\,(s)$, $T_{MT2} = 1.73\,(s)$, $T_{MT3} = 1.21\,(s)$. *These results clearly indicate that the proposed method (MT3) exhibits the fastest convergence among the three approaches. Additionally, Figure 1 provides a visual comparison, highlighting the significantly improved convergence speed of the proposed method (MT3) relative to MT1 and MT2. This superior performance underscores the efficiency and effectiveness of the proposed approach in achieving rapid stabilization.*

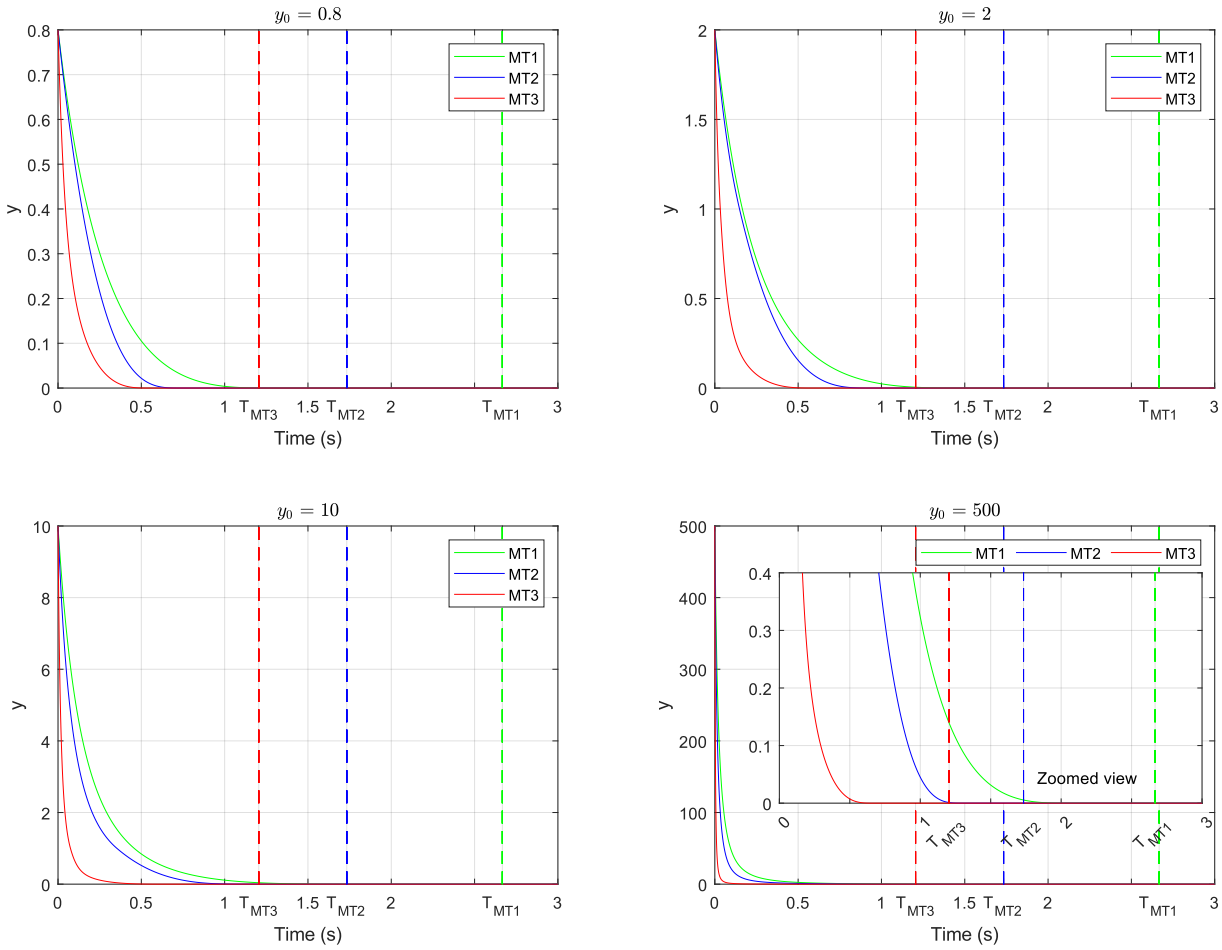

Figure 1. Comparison of convergence behavior across fixed-time control methods under different initial conditions.

3.2. Dynamic Model Approximation Using Time-Delay Estimation

The dynamic model of n-joint robot arms is articulated as follows:

$$J(\alpha)\ddot{\alpha} + V(\alpha, \dot{\alpha})\dot{\alpha} + \tau_G(\alpha) + \tau_F(\dot{\alpha}) = \tau - \tau_d, \tag{25}$$

where $\alpha \in \mathbb{R}^n$ signifies the joint position vector, $\dot{\alpha} \in \mathbb{R}^n$ and $\ddot{\alpha} \in \mathbb{R}^n$ represent the vectors of angular velocity and acceleration, respectively. $J(\alpha) \in \mathbb{R}^{n\times n}$ denotes the inertia matrix, while $V(\alpha, \dot{\alpha}) \in \mathbb{R}^{n\times n}$ describes the matrix of centrifugal and Coriolis forces. $\tau_G(\alpha) \in \mathbb{R}^n$ represents the gravity vector, and the friction force is denoted by the vector $\tau_F(\dot{\alpha}) \in \mathbb{R}^n$. External disturbances are accounted for in the vector $\tau_d \in \mathbb{R}^n$, while the control input torque is denoted as $\tau \in \mathbb{R}^n$.

With a positive diagonal gain matrix $\bar{J} \in \mathbb{R}^{n\times n}$, Equation (25) can be rewritten as:

$$\bar{J}\ddot{\alpha} + W(\alpha, \dot{\alpha}, \ddot{\alpha}) = \tau, \tag{26}$$

where $W(\alpha, \dot{\alpha}, \ddot{\alpha}) = (J(\alpha) - \bar{J})\ddot{\alpha} + V(\alpha, \dot{\alpha})\dot{\alpha} + \tau_G(\alpha) + \tau_F(\dot{\alpha}) + \tau_d \in \mathbb{R}^n$ encapsulates all the dynamic model components and uncertainty terms.

Accurately computing the complete dynamic model of a robotic manipulator and its uncertainties is often challenging. This difficulty arises from factors such as a high degree of freedom, the manipulator's complex structure, and unknown uncertainties. To address these challenges, this study employs a practical technique called TDE. TDE approximates the value of $W(\alpha, \dot{\alpha}, \ddot{\alpha})$ by utilizing past state values of the control input and acceleration.

The estimation of $W(\alpha, \dot{\alpha}, \ddot{\alpha})$ is given by [40–42]:

$$\hat{W}_t \triangleq W_{t-K} = \tau_{t-K} - \bar{J}\ddot{\alpha}_{t-K}, \tag{27}$$

where $\bullet_{t-K}$ denotes the time-delayed value of $\bullet$, and K is a small time delay, often chosen as the sampling time. The delayed acceleration term $\ddot{\alpha}_{t-K}$ is computed as:

$$\ddot{\alpha}_{t-K} = \begin{cases} 0 & \text{if } t \leq T, \\ \frac{\alpha_t - 2\alpha_{t-K} + \alpha_{t-2K}}{K^2} & \text{if } t > T, \end{cases} \tag{28}$$

where $T \geq 2K$. The value of T should not be excessively large to maintain accuracy.

Using Equation (28) effectively mitigates the pronounced fluctuations observed in the early stages of $\ddot{\alpha}_{t-K}$. As a result, the TDE method achieves accurate estimation with relatively small and bounded errors [43].

For $K \approx 0$, the TDE error, defined as $\Delta W = W - \hat{W}_t$, remains small and bounded. The magnitude of the estimation error is influenced by K and satisfies:

$$\|\Delta W\| \leq \overline{\Delta W}, \tag{29}$$

where $\overline{\Delta W}$ is a positive constant.

Remark 2. *The TDE error ΔW can be effectively bounded, as shown in Equation (29), provided that the matrix $\bar{J}$ is selected to satisfy the condition $\|I - J^{-1}(\alpha)\bar{J}\| < 1$. This condition ensures that the approximation error introduced by the TDE remains within acceptable limits. Furthermore, as detailed in [40–42], the validity of this bound is well-supported for sufficiently small values of K, making it a practical and reasonable assumption for ensuring the robustness and stability of the proposed control strategy.*

The position and velocity tracking errors are defined as $e = \alpha - \alpha_d$ and $\dot{e} = \dot{\alpha} - \dot{\alpha}_d$, respectively, where α_d represents the desired trajectory. Consequently, Equation (26) can be reformulated in the error space as:

$$\ddot{e} = \bar{J}^{-1}\left(\tau - \hat{W}_t + \Delta W\right) - \ddot{\alpha}_d, \tag{30}$$

where $\bar{J}$ is the positive diagonal matrix, τ denotes the control input, $\hat{W}_t$ is the estimated dynamics, and ΔW is the estimation error.

3.3. Design of the Novel Auxiliary System for Input Saturation

To mitigate the effects of actuator saturation, a novel auxiliary system is proposed by:

$$\dot{\gamma} = -\bar{J}^{-1}\xi\gamma - \bar{J}^{-1}\bar{\xi}\text{sign}(\gamma) - P_{ST}(\gamma)(m_3[\gamma]^{n_3} + m_4[\gamma]^{n_4}) + \bar{J}^{-1}\Delta\tau, \tag{31}$$

where $P_{ST}(\gamma) = \text{diag}\left(\frac{1}{P(\gamma_1)}, \ldots, \frac{1}{P(\gamma_n)}\right)$, and the components of $P(\gamma_i)$ are expressed as:

$$P(\gamma_i) = a_1 + \frac{1 - a_1}{1 + r_1|\gamma_i|^{h_1}},$$

with $0 < a_1 < 1$, $r_1 > 0$, and h_1 is an even positive integer. Consequently, we have $0 < P(\gamma_i) \leq 1$. $\xi = \text{diag}(\xi_1, \ldots, \xi_n)$, $\bar{\xi} = \text{diag}(\bar{\xi}_1, \ldots, \bar{\xi}_n)$, $m_3 = \text{diag}(m_{31}, \ldots, m_{3n})$, $m_4 = \text{diag}(m_{41}, \ldots, m_{4n})$ are positive diagonal matrices, and $\overline{\Delta\tau} > 0$. The exponents $n_3 = [n_{31}, \ldots, n_{3n}]^T$ and $n_4 = [n_{41}, \ldots, n_{4n}]^T$ are defined as $n_{3i} = l_3^{\text{sign}(|\gamma_i|-1)}$ and $n_{4i} = l_4^{\text{sign}(1-|\gamma_i|)}$, where $l_3 > 1$ and $0.5 < l_4 < 1$.

The term $\Delta\tau$ represents the mismatch between the actual control input and the saturated actuator output. It is expressed as:

$$\Delta\tau = \tau_{\text{SAT}} - \tau, \tag{32}$$

where $\Delta\tau$ is bounded by $\|\Delta\tau\| < \overline{\Delta\tau}$.

The saturated actuator output τ_{SAT} is defined by:

$$\tau_{\text{SAT}} = \begin{cases} \tau_{\max} & \text{if } \tau \geq \tau_{\max}, \\ \tau & \text{if } \tau_{\min} < \tau < \tau_{\max}, \\ \tau_{\min} & \text{if } \tau \leq \tau_{\min}, \end{cases} \tag{33}$$

where $\tau_{\min} < 0$ and $\tau_{\max} > 0$ denote the lower and upper saturation limits of the actuator, respectively.

To analyze the stability of the system (31), consider the Lyapunov candidate function $V_1 = 0.5\gamma^T\gamma$. By differentiating V_1 and substituting the auxiliary system dynamics from Equation (31), we obtain:

$$\begin{aligned} \dot{V}_1 &= \gamma^T\dot{\gamma} \\ &= \gamma^T\left[-\bar{J}^{-1}\xi\gamma - \bar{J}^{-1}\bar{\xi}\text{sign}(\gamma) - P_{ST}(\gamma)(m_3[\gamma]^{n_3} + m_4[\gamma]^{n_4}) + \bar{J}^{-1}\Delta\tau\right] \\ &= \sum_{i=1}^{n}\frac{1}{\bar{J}_i}\left(\Delta\tau_i\gamma_i - \xi_i\gamma_i^2 - \bar{\xi}_i|\gamma_i|\right) - \sum_{i=1}^{n}\frac{1}{P(\gamma_i)}\left(m_3|\gamma_i|^{n_{3i}+1} + m_4|\gamma_i|^{n_{4i}+1}\right) \\ &\leq \sum_{i=1}^{n}\frac{1}{\bar{J}_i}\left(\Delta\tau_i - \xi_i\gamma_i - \bar{\xi}_i\right)|\gamma_i| - \sum_{i=1}^{n}\frac{1}{P(\gamma_i)}\left(m_3|\gamma_i|^{n_{3i}+1} + m_4|\gamma_i|^{n_{4i}+1}\right). \end{aligned} \tag{34}$$

By choosing ξ_i to be sufficiently large, the term $-\xi_i\gamma_i$ dominates $\Delta\tau_i$, ensuring $\Delta\tau_i - \xi_i\gamma_i \leq \bar{\xi}_i$. Substituting this condition into Equation (34) further simplifies it to:

$$\dot{V}_1 \leq -\sum_{i=1}^{n}\left(m_3|\gamma_i|^{n_{3i}+1} + m_4|\gamma_i|^{n_{4i}+1}\right). \tag{35}$$

The stability analysis is performed under two distinct cases based on the magnitude of $|\gamma_i|$:

Case 1: $|\gamma_i| \geq 1$

In this scenario, $n_{3i} = l_3 > 1$ and $n_{4i} = l_4^{-1} > 1$. Therefore:

$$m_{3i}|\gamma_i|^{n_{3i}+1} + m_{4i}|\gamma_i|^{n_{4i}+1} = m_{3i}\left(|\gamma_i|^2\right)^{\frac{l_3+1}{2}} + m_{4i}\left(|\gamma_i|^2\right)^{\frac{l_4^{-1}+1}{2}}. \tag{36}$$

Given that $\frac{l_4^{-1}+1}{2} > 1 > \frac{l_4+1}{2}$ and $|\gamma_i|^2 > 1$, it follows that:

$$\left(|\gamma_i|^2\right)^{\frac{l_4^{-1}+1}{2}} > \left(|\gamma_i|^2\right)^{\frac{l_4+1}{2}}. \tag{37}$$

Thus, the inequality can be bounded as:

$$m_{3i}|\gamma_i|^{n_{3i}+1} + m_{4i}|\gamma_i|^{n_{4i}+1} > m_{3i}\left(|\gamma_i|^2\right)^{\omega_3} + m_{4i}\left(|\gamma_i|^2\right)^{\omega_4}, \tag{38}$$

where $\omega_3 = \frac{l_3+1}{2}$ and $\omega_4 = \frac{l_4+1}{2}$.

Case 2: $|\gamma_i| < 1$

In this case, $n_{3i} = l_3^{-1} < 1$ and $n_{4i} = l_4 < 1$. Consequently:

$$m_{3i}|\gamma_i|^{n_{3i}+1} + m_{4i}|\gamma_i|^{n_{4i}+1} = m_{3i}\left(|\gamma_i|^2\right)^{\frac{l_3^{-1}+1}{2}} + m_{4i}\left(|\gamma_i|^2\right)^{\frac{l_4+1}{2}}. \tag{39}$$

Since $\frac{l_3^{-1}+1}{2} < 1 < \frac{l_3+1}{2}$ and $|\gamma_i|^2 < 1$, we have:

$$\left(|\gamma_i|^2\right)^{\frac{l_3^{-1}+1}{2}} > \left(|\gamma_i|^2\right)^{\frac{l_3+1}{2}}. \tag{40}$$

Thus, the inequality can again be bounded as:

$$m_{3i}|\gamma_i|^{n_{3i}+1} + m_{4i}|\gamma_i|^{n_{4i}+1} > m_{3i}\left(|\gamma_i|^2\right)^{\omega_3} + m_{4i}\left(|\gamma_i|^2\right)^{\omega_4}. \tag{41}$$

From the above cases, the derivative of V_1 can be represented as:

$$\dot{V}_1 \leq -\sum_{i=1}^{n}\left(m_{3i}\left(|\gamma_i|^2\right)^{\omega_3} + m_{4i}\left(|\gamma_i|^2\right)^{\omega_4}\right). \tag{42}$$

Using minimum eigenvalues, we write:

$$\dot{V}_1 \leq -\lambda_{\min}(m_3)\sum_{i=1}^{n}\left(|\gamma_i|^2\right)^{\omega_3} - \lambda_{\min}(m_4)\sum_{i=1}^{n}\left(|\gamma_i|^2\right)^{\omega_4}. \tag{43}$$

Applying Lemma 3, this simplifies further to:

$$\dot{V}_1 \leq -\bar{m}_3 V_1^{\omega_3} - \bar{m}_4 V_1^{\omega_4}, \tag{44}$$

where $\bar{m}_3 = n^{1-\omega_3}\lambda_{\min}(m_3)2^{\omega_3}$ and $\bar{m}_4 = \lambda_{\min}(m_4)2^{\omega_4}$.

Using Equation (44) and Lemma 1, the state γ converges to zero within a fixed time. The settling time is given by:

$$T_c < \frac{1}{\bar{m}_3(\omega_3 - 1)} + \frac{1}{\bar{m}_4(1 - \omega_4)}. \tag{45}$$

Finally, by defining $\varphi_1 = e$ and $\varphi_2 = \dot{e} - \gamma$, the auxiliary system transforms into:

$$\begin{cases} \dot{\varphi}_1 = \varphi_2 + \gamma \\ \dot{\varphi}_2 = \bar{J}^{-1}(\tau_{\mathrm{SAT}} - \hat{W}_t + \Delta W_t) - \ddot{\alpha}_d + \bar{J}^{-1}\xi\gamma + \bar{J}^{-1}\bar{\xi}\mathrm{sign}(\gamma) \\ \quad\quad +P_{ST}(\gamma)\left(m_3[\gamma]^{n_3} + m_4[\gamma]^{n_4}\right) - \bar{J}^{-1}\Delta\tau \end{cases} \tag{46}$$

3.4. Design of the Novel NFTSM Surface

The novel NFTSM surface is formulated based on the proposal in Theorem 1 as:

$$S_i = \begin{cases} \varphi_{2i} + P^{-1}(\varphi_{1i})(m_{5i}[\varphi_{1i}]^{n_{5i}} + m_{6i}[\varphi_{1i}]^{n_{6i}}), & \text{if } \bar{S}_i = 0 \text{ or } (\bar{S}_i \neq 0 \text{ and } |\varphi_{1i}| > \chi), \\ \varphi_{2i} + P^{-1}(\varphi_{1i})\left(\varepsilon_{5i}\varphi_{1i} + \varepsilon_{6i}[\varphi_{1i}]^2\right), & \text{if } \bar{S}_i \neq 0 \text{ and } |\varphi_{1i}| \leq \chi, \end{cases} \tag{47}$$

where $\bar{S}_i = \varphi_{2i} + P^{-1}(\varphi_{1i})(m_{5i}[\varphi_{1i}]^{n_{5i}} + m_{6i}[\varphi_{1i}]^{n_{6i}})$, $P(\varphi_{1i}) = a_2 + \frac{(1-a_2)}{1+r_2|\varphi_{1i}|^{h_2}} \leq 1$, with $0 < a_2 < 1$, $r_2 > 0$, and h_2 being an even positive integer. The parameters m_{5i} and m_{6i} satisfy $m_{5i} > 0$ and $m_{6i} > 0$, while the constants $l_5 > 1$ and $0.5 < l_6 < 1$ govern the exponents $n_{5i} = l_5^{\mathrm{sign}(|\varphi_{1i}|-1)}$ and $n_{6i} = l_6^{\mathrm{sign}(1-|\varphi_{1i}|)}$. Additionally, $\varepsilon_{5i} = m_{5i}(2 - n_{5i})\chi^{n_{5i}-1} + m_{6i}(2 - n_{6i})\chi^{n_{6i}-1}$, $\varepsilon_{6i} = m_{5i}(n_{5i} - 1)\chi^{n_{5i}-2} + m_{6i}(n_{6i} - 1)\chi^{n_{6i}-2}$, and $\chi > 0$ is a small positive constant.

Once the sliding mode condition ($S_i = 0$) is satisfied, and when $\bar{S}_i = 0$ or ($\bar{S}_i \neq 0$ and $|\varphi_{1i}| > \chi$), the system behavior reduces to:

$$\varphi_{2i} = -P^{-1}(\varphi_{1i})(m_{5i}[\varphi_{1i}]^{n_{5i}} + m_{6i}[\varphi_{1i}]^{n_{6i}}), \tag{48}$$

After time T_c, it is assumed that $\gamma = 0$. Therefore, Equation (48) simplifies further to:

$$\dot{\varphi}_{1i} = -P^{-1}(\varphi_{1i})(m_{5i}[\varphi_{1i}]^{n_{5i}} + m_{6i}[\varphi_{1i}]^{n_{\varphi_{1i}}}), \tag{49}$$

This equation conforms to the structure described in Theorem 1, ensuring that φ_1 converges to zero within a fixed time $T_s = \max\{T_{si}\}$, where T_{si} is determined as follows:

$$\begin{aligned} T_{si} = &\min\left\{ \frac{\bar{a}_2}{(l_5 - 1)m_{6i}} \ln\left(1 + \frac{m_{6i}}{m_{5i}}\right), \frac{l_6\bar{a}}{(1 - l_6)m_{5i}} \ln\left(1 + \frac{m_{5i}}{m_{6i}}\right) \right\} \\ &+ \min\left\{ \frac{1}{(1 - l_6)m_{5i}} \ln\left(1 + \frac{m_{5i}}{m_{6i}}\right), \frac{l_5}{(l_5 - 1)m_{6i}} \ln\left(1 + \frac{m_{6i}}{m_{5i}}\right) \right\} \end{aligned} \tag{50}$$

When $\bar{S}_i \neq 0$ and $|\varphi_{1i}| \leq \chi$, the system transitions from a fixed-time sliding mode to a general sliding mode as described in Figure 2. The design of the general sliding mode surface ensures the continuity of S_i and its derivative, the mitigation of singularity issues inherent in classical TSMC designs [44]. Since $\varphi_1 = e$, the tracking error e is guaranteed to converge within a small bound χ in a fixed time T_s.

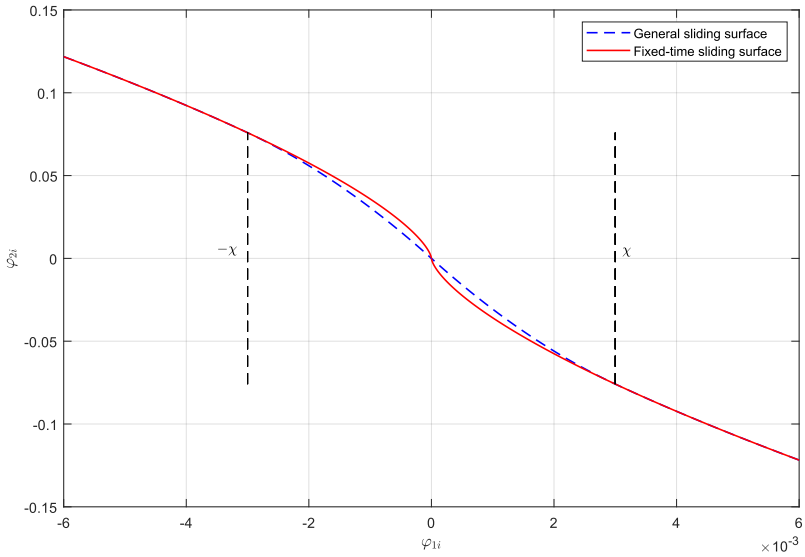

Figure 2. Proposed sliding surface.

3.5. Design of the Proposed Control Law

Taking the time derivative of the sliding mode surface S and utilizing Equation (46), the expression becomes:

$$\begin{aligned}\dot{S} = \bar{J}^{-1}(\tau - \hat{W}_t + \Delta W) - \ddot{\alpha}_d + \bar{J}^{-1}\xi\gamma + \bar{J}^{-1}\bar{\xi}\mathrm{sign}(\gamma) \\ + P_{ST}(\gamma)(\varepsilon_3[\gamma]^{n_3} + \varepsilon_4[\gamma]^{n_4}) + \Psi,\end{aligned} \tag{51}$$

where $\Psi = [\Psi_1, \ldots, \Psi_n]^T$, and each component Ψ_i is defined as:

$$\Psi_i = \begin{cases} P^{-1}(\varphi_{1i})\left(n_{5i}m_{5i}|\varphi_{1i}|^{n_{5i}-1} + n_{6i}m_{6i}|\varphi_{1i}|^{n_{6i}-1}\right)\dot{\varphi}_{1i} \\ \quad - P^{-2}(\varphi_{1i})\dot{P}(\varphi_{1i})\left(m_{5i}|\varphi_{1i}|^{n_{5i}} + m_{6i}|\varphi_{1i}|^{n_{6i}}\right), & \text{if } \bar{S}_i = 0 \text{ or } (\bar{S}_i \neq 0 \text{ and } |\varphi_{1i}| > \chi), \\ P^{-1}(\varphi_{1i})\left(\varepsilon_{5i} + 2\varepsilon_{6i}|\varphi_{1i}|\right)\dot{\varphi}_{1i} \\ \quad - P^{-2}(\varphi_{1i})\dot{P}(\varphi_{1i})\left(\varepsilon_{5i}\varphi_{1i} + \varepsilon_{6i}|\varphi_{1i}|^2\right), & \text{if } \bar{S}_i \neq 0 \text{ and } |\varphi_{1i}| \leq \chi. \end{cases}$$

Here, $\dot{P}(\varphi_{1i})$ is expressed as $\dot{P}(\varphi_{1i}) = (a_2 - 1)r_2h_2|\varphi_{1i}|^{h_2-1}\,\mathrm{sign}(\varphi_{1i})\dot{\varphi}_{1i}/\left(1 + r_2|\varphi_{1i}|^{h_2}\right)^2$.

Based on Equation (51), the proposed model-free fixed-time NFTSMC law is designed as follows:

$$\begin{cases} \tau = \tau_{\mathrm{eq}} + \tau_{\mathrm{r}}, \\ \tau_{\mathrm{eq}} = \hat{W}_t + \bar{J}\left(\ddot{\alpha}_d - \bar{J}^{-1}\xi\gamma - \bar{J}^{-1}\bar{\xi}\mathrm{sign}(\gamma) - P_{ST}(\gamma)\left(m_3[\gamma]^{n_3} + m_4[\gamma]^{n_4}\right) - \Psi\right), \\ \tau_{\mathrm{r}} = -\overline{\Delta W}\,\mathrm{sign}(S) - P_R(S)\left(m_7[S]^{n_7} + m_8[S]^{n_8}\right), \end{cases} \tag{52}$$

where τ_{eq} represents the equivalent control law, and τ_{r} is the novel FTRCL designed according to the proposal outlined in Theorem 1. The term $P_R(S) = \mathrm{diag}(1/P(S_1), \ldots, 1/P(S_n))$ is a diagonal positive definite matrix, with its elements $P(S_i) = a_3 + (1 - a_3)/(1 + r_3|S_i|^{h_3})$, ensuring that $0 < P(S_i) \leq 1$. The parameters a_3 and r_3 are positive scalars, with $0 < a_3 < 1$, while h_3 is an even positive integer. The coefficients $m_7 = \mathrm{diag}(m_{71}, \ldots, m_{7n})$ and $m_8 = \mathrm{diag}(m_{81}, \ldots, m_{8n})$ are diagonal matrices with positive entries. The exponents $n_7 = [n_{71}, \ldots, n_{7n}]$ and $n_8 = [n_{81}, \ldots, n_{8n}]$ are adaptive, defined as $n_{7i} = l_7^{\mathrm{sign}(|S_i|-1)}$ and $n_{8i} = l_8^{\mathrm{sign}(1-|S_i|)}$, where $l_7 > 1$ and $0.5 < l_8 < 1$.

The structure of the proposed control system is depicted in Figure 3.

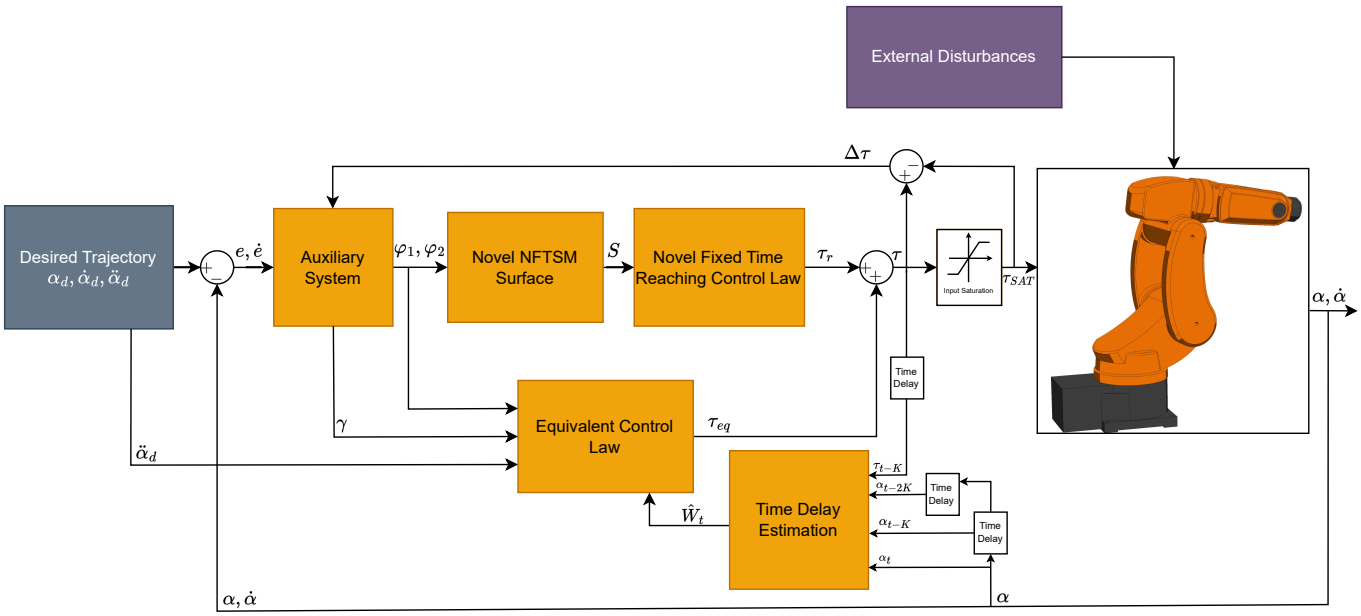

Figure 3. Structure of the proposed control system.

3.6. Stability Analysis

Substituting the proposed control law from Equation (52) into Equation (51) yields:

$$\dot{S} = \bar{J}^{-1}\left(\Delta W - \overline{\Delta W}\,\mathrm{sign}(S) - P_R(S)\left(m_7[S]^{n_7} + m_8[S]^{n_8}\right)\right). \tag{53}$$

To analyze the stability, consider the Lyapunov candidate function $V_2 = 0.5S^TS$. Taking its time derivative and substituting Equation (53) leads to:

$$\begin{aligned}
\dot{V}_2 &= S^T\dot{S} \\
&= S^T\bar{J}^{-1}\left(\Delta W - \overline{\Delta W}\,\mathrm{sign}(S) - P_R(S)\left(m_7[S]^{n_7} + m_8[S]^{n_8}\right)\right) \\
&= \sum_{i=1}^{n} J_i^{-1}\left(\Delta W_i S_i - \overline{\Delta W}|S_i| - P^{-1}(S_i)\left(m_{7i}|S_i|^{n_{7i}+1} + m_{8i}|S_i|^{n_{8i}+1}\right)\right) \\
&\le \sum_{i=1}^{n} J_i^{-1}\left(\Delta W_i - \overline{\Delta W}\right)|S_i| - \sum_{i=1}^{n} J_i^{-1}P^{-1}(S_i)\left(m_{7i}|S_i|^{n_{7i}+1} + m_{8i}|S_i|^{n_{8i}+1}\right) \\
&\le -\sum_{i=1}^{n} J_i^{-1}\left(m_{7i}|S_i|^{n_{7i}+1} + m_{8i}|S_i|^{n_{8i}+1}\right).
\end{aligned} \tag{54}$$

Following the analysis in Equation (35), Equation (54) can be reformulated as:

$$\begin{aligned}
\dot{V}_2 &\le -\sum_{i=1}^{n} J_i^{-1}\left(m_{7i}\left(|S_i|^2\right)^{\omega_7} + m_{8i}\left(|S_i|^2\right)^{\omega_8}\right) \\
&\le -\lambda_{\max}^{-1}(J)\lambda_{\min}(m_7)\sum_{i=1}^{n}\left(|S_i|^2\right)^{\omega_7} - \lambda_{\max}^{-1}(J)\lambda_{\min}(m_8)\sum_{i=1}^{n}\left(|S_i|^2\right)^{\omega_8},
\end{aligned} \tag{55}$$

where $\omega_7 = \frac{l_7+1}{2}$ and $\omega_8 = \frac{l_8+1}{2}$.

Using Lemma 3, Equation (55) can be rewritten as:

$$\begin{aligned}\dot{V}_2 &\leq -n^{1-\omega_7}\lambda_{\max}^{-1}(J)\lambda_{\min}(m_7)2^{\omega_7}\left(0.5\sum_{i=1}^{n}|S_i|^2\right)^{\omega_7} \\ &\quad -\lambda_{\max}^{-1}(J)\lambda_{\min}(m_8)2^{\omega_8}\left(0.5\sum_{i=1}^{n}|S_i|^2\right)^{\omega_8} \\ &\leq -\bar{m}_7 V_2^{\omega_7} - \bar{m}_8 V_2^{\omega_8},\end{aligned} \tag{56}$$

where $\bar{m}_7 = n^{1-\omega_7}\lambda_{\max}^{-1}(J)\lambda_{\min}(m_7)2^{\omega_7}$ and $\bar{m}_8 = \lambda_{\max}^{-1}(J)\lambda_{\min}(m_8)2^{\omega_8}$.

From Equation (56) and Lemma 1, it follows that the sliding surface S converges to zero within a fixed time. The settling time T_r is given by:

$$T_r < \frac{1}{\bar{m}_7(\omega_7 - 1)} + \frac{1}{\bar{m}_8(1-\omega_8)}. \tag{57}$$

Therefore, the total convergence time is bounded by the sum $T_s + T_r + T_c$.

4. Numerical Simulation and Discussion

To assess the effectiveness of the proposed control method, numerical simulations were conducted in the MATLAB/SIMULINK-2021b environment for a 3-DOF SAMSUNG FARA AT2 robot manipulator. The mechanical model of the manipulator was meticulously designed in SOLIDWORKS-2018 software, as illustrated in Figure 4. This model was then integrated into the SIMULINK simulation environment using the SIMSCAPE MULTI-BODY LINK tool, ensuring that the simulation closely mirrored the actual robotic system. The robot's parameters are detailed in our previous study [5]. The sampling time for the simulations was set to 10^{-3} s, ensuring high fidelity in dynamic response analysis.

To highlight the advantages of the proposed control method, its performance was benchmarked against several well-established approaches, including NTSMC [45], NFTSMC (based on [46]), and global NTSMC (GNTSMC) (based on [47]).

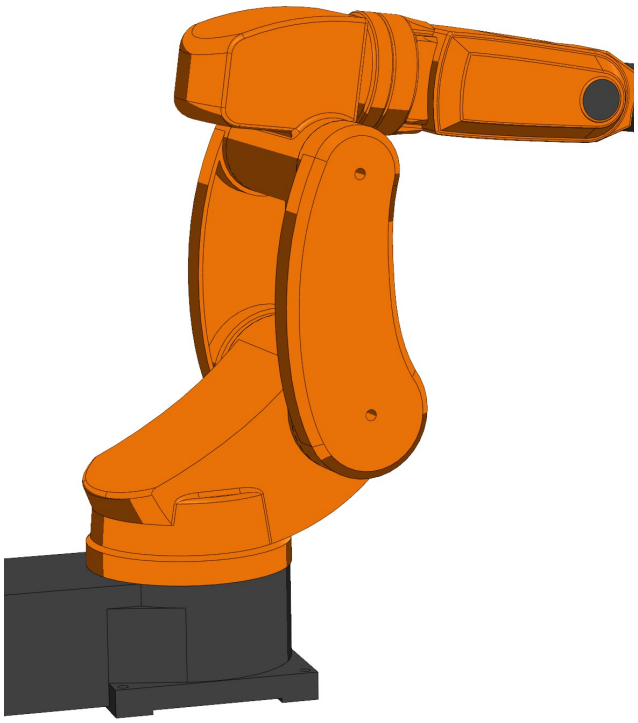

Figure 4. Three-dimensional SOLIDWORKS model of SAMSUNG FARA AT2 manipulator.

The control law for NTSMC [45] is given by:

$$s = \ell + \mathrm{H}\dot{e}^{\frac{\varsigma_1}{\varsigma_2}}, \tag{58}$$

$$\ell = \left[\left(1+e_1^2\right)^{\frac{\varsigma_1}{\varsigma_2}} \arctan(e_1), \ldots, \left(1+e_n^2\right)^{\frac{\varsigma_1}{\varsigma_2}} \arctan(e_n)\right]^T, \tag{59}$$

$$\tau = J_0(\ddot{\alpha}_d - \mathrm{M}) + V_0(\alpha,\dot{\alpha})\dot{\alpha} + \tau_{G0}(\alpha) - J_0(\kappa_1 \mathrm{sign}(s) + \kappa_2 s), \tag{60}$$

$$\mathrm{M} = \left[\frac{\varsigma_2(1+e_1^2)^{\frac{\varsigma_1}{\varsigma_2}-1}\dot{e}_1^{2-\frac{\varsigma_1}{\varsigma_2}}}{H_1\varsigma_1}\left(1+\frac{2\varsigma_1 e_1 \arctan(e_1)}{\varsigma_2}\right), \quad \ldots, \quad \frac{\varsigma_2(1+e_n^2)^{\frac{\varsigma_1}{\varsigma_2}-1}\dot{e}_n^{2-\frac{\varsigma_1}{\varsigma_2}}}{H_n\varsigma_1}\left(1+\frac{2\varsigma_1 e_n \arctan(e_n)}{\varsigma_2}\right)\right]^T. \tag{61}$$

Here, H, κ_1, and κ_2 are positive diagonal matrices, ς_1 and ς_2 are positive odd constants, and $1 < \frac{\varsigma_1}{\varsigma_2} < 2$.

The NFTSMC law [46] is formulated as:

$$s = e + \mathrm{K}[e]^{\hbar_1} + \mathrm{T}\dot{e}^{\hbar_2}, \tag{62}$$

$$\tau = J_0(\ddot{\alpha}_d - \mathrm{P}) + V_0(\alpha,\dot{\alpha})\dot{\alpha} + \tau_{G0}(\alpha) - J_0(\kappa_1 \mathrm{sign}(s) + \kappa_2 s), \tag{63}$$

$$\mathrm{P} = \left[\frac{[\dot{e}_1]^{2-\hbar_2}}{\hbar_2 \mathrm{T}_1}\left(1+\mathrm{K}_1|e_1|^{\hbar_1-1}\right), \ldots, \frac{[\dot{e}_n]^{2-\hbar_2}}{\hbar_2 \mathrm{T}_n}\left(1+\mathrm{K}_n|e_n|^{\hbar_1-1}\right)\right]^T. \tag{64}$$

Here, K, T, κ_1, and κ_2 are positive diagonal matrices, with $1 < \hbar_2 < 2$ and $\hbar_1 > \hbar_2$.

The control law for GNTSMC [47] is constructed as follows:

$$s_i = e_i + \rho_{1i}[e_i]^{z_{1i}} + \rho_{2i}[\dot{e}_i]^{z_{2i}(t)} + g_i(t), \tag{65}$$

$$g_i(t) = \begin{cases} g_{1i} + g_{2i}t - \left(\frac{3g_{1i}}{\bar{t}^2} + \frac{2g_{2i}}{\bar{t}^2}\right)t^2 + \left(\frac{2g_{1i}}{\bar{t}^3} + \frac{g_{2i}}{\bar{t}^3}\right)t^3, & \text{if } t \le \bar{t}, \\ 0, & \text{if } t > \bar{t}, \end{cases} \tag{66}$$

$$\begin{aligned} g_{1i} &= e_i(0) + \rho_{1i}[e_i(0)]^{z_{1i}} + \rho_{2i}[\dot{e}_i(0)]^{z_{2i}(t)}, \\ g_{2i} &= \dot{e}_i(0) + z_{1i}\rho_{1i}|e_i(0)|^{z_{1i}-1}\dot{e}_i(0) + z_{2i}\rho_{2i}|\dot{e}_i(0)|^{z_{2i}(t)-1}\ddot{e}_i(0) \\ &\quad + \rho_{2i}\dot{z}_{2i}[\dot{e}_i(0)]^{z_{2i}(t)}\ln(|\dot{e}_i(0)|), \end{aligned} \tag{67}$$

$$z_{2i}(t) = \begin{cases} 1, & \text{if } t \le \bar{t}, \\ 1 + t - \bar{t}, & \text{if } \bar{t} < t \le \bar{t} + \Xi, \\ 1 + \Xi, & \text{if } t > \bar{t} + \Xi, \end{cases} \tag{68}$$

$$\tau = J_0(\ddot{\alpha}_d - \Pi) + V_0(\alpha,\dot{\alpha})\dot{\alpha} + \tau_{G0}(\alpha) - J_0\left(\hat{\kappa}_3[s]^{1/2} + \int \hat{\kappa}_4 \,\mathrm{sign}(s)\right), \tag{69}$$

$$\begin{aligned} \Pi_i &= z_{2i}^{-1}(t)\rho_{2i}^{-1}\left(1+\rho_{1i}|e_i|^{z_{1i}-1}\right)|\dot{e}_i|^{2-z_{2i}(t)}\,\mathrm{sign}(\dot{e}_i) \\ &\quad + z_{2i}^{-1}(t)\rho_{2i}^{-1}|\dot{e}_i|^{1-z_{2i}(t)}\dot{g}_i(t) + \dot{z}_{2i}(t)z_{2i}^{-1}(t)\dot{e}_i\ln(|\dot{e}_i|), \end{aligned} \tag{70}$$

$$\begin{aligned} \hat{\kappa}_3 &= \bar{\kappa}_3\zeta, \\ \hat{\kappa}_4 &= \bar{\kappa}_4\zeta, \\ \dot{\zeta} &= \mathrm{diag}\left(\sqrt{\frac{L}{2}}\,\mathrm{sign}(|s|)\right), \end{aligned} \tag{71}$$

where $\rho_{1i} > 0$, $\rho_{2i} > 0$, $z_{1i} \ge 2$, $\bar{t} > 0$ and $0 < \Xi < 1$. $\bar{\kappa}_3$, $\bar{\kappa}_4$ and L are positive diagonal matrices with $\bar{\kappa}_{4i} = 0.25\bar{\kappa}_{3i}z_{2i}(t)\rho_{2i}|\dot{e}_i|^{z_{2i}(t)-1}$.

The desired trajectory of the robot end-effector is defined as $X_d = 0.43 + 0.02\sin(t)$, $Y_d = 0.1\sin(t)$, $Z_d = 0.260 + 0.1\cos(0.5t)$. Using inverse kinematics, the desired joint trajectories are calculated and provided as input to the controllers.

To replicate realistic operating conditions, joint friction is modeled as $\tau_F = [2\dot{\phi}_1 + 0.01\text{sign}(\dot{\phi}_1), 2\dot{\phi}_2 + 0.01\text{sign}(\dot{\phi}_2), 2\dot{\alpha}_3 + 0.01\text{sign}(\dot{\alpha}_3)]^T$. This model accounts for both viscous and Coulomb friction, adding complexity to the control task.

External disturbances are introduced to test the robustness of the controllers. The disturbances are defined as $\tau_d = [-2\sin(0.5t) - 2\sin(t), 2\sin(0.5t) + 1.5\sin(0.75t), -1.5\sin(0.5t) - 0.8\sin(0.25t)]^T$, simulating dynamic and time-varying external forces acting on the robot's joints.

Uncertainties in the robot's dynamic model are incorporated by modifying the nominal parameters. Specifically, the inertia matrix, Coriolis forces, and gravitational forces are scaled as $J_0 = 0.85J$, $V_0 = 0.85V$, and $\tau_{G0} = 0.85\tau_G$, respectively. These modifications ensure that the simulation reflects potential discrepancies between the actual and nominal models, challenging the controllers' adaptability.

The joint actuators are subjected to input saturation limits. The saturation bounds are set as $\tau_{\min} = [-35, -55, -30]$ (N.m) and $\tau_{\max} = [35, 55, 30]$ (N.m). These constraints mimic real-world actuator limitations and test the controllers' ability to maintain performance within bounded inputs.

The control parameters for all methods are summarized in Table 1. From the control parameters, we can calculate the theoretical convergence time of the proposed method as $T_{\max} = T_s + T_r + T_c = 0.97 + 1.28 + 2.96 = 5.21$ (s).

Table 1. Parameters of control methods.

Methods	**Parameters**	**Values**
NTSMC	H, κ_1, κ_2, ς_1, ς_2	diag(0.3,0.3,0.3), diag(14,14,14), diag(5,5,5), 7, 5
NFTSMC	K, T, κ_1, κ_2, $\hbar_1$, $\hbar_2$	diag(5,5,5), diag(0.3,0.3,0.3), diag(14,14,14), diag(5,5,5), 1.61, 7/5
GNTSMC	ρ_{1i}, ρ_{2i}, z_{1i}, $\bar{t}$, Ξ, $\bar{\kappa}_{3i}$, L_i	5, 0.1, 2, 0.05, 0.5, 20, 5000
Proposed Method	$\bar{J}, \xi_i, \bar{\xi}_i$	diag(0.4,0.4,0.2), 50, 0.001
	m_{3i}, m_{4i}, l_3, l_4, a_1, r_1, h_1	2, 2, 1.5, 0.7, 0.4, 5, 2
	m_{5i}, m_{6i}, l_5, l_6, a_2, r_2, h_2, χ	5, 5, 1.25, 0.8, 0.4, 5, 2, 0.00001
	m_{7i}, m_{8i}, l_7, l_8, a_3, r_3, h_3, $\overline{\Delta W}$	3, 3, 1.25, 0.8, 0.3, 100, 4, 0.008

Remark 3. *The parameters of the proposed control method were chosen following the guidelines provided in the paper. The selection and tuning of these parameters play a critical role in shaping the system's performance and convergence properties. The effects of the parameters can be summarized as follows:*

- *High values of $m_{3i}, m_{4i}, m_{5i}, m_{6i}, m_{7i}, m_{8i}$: Increasing these parameters enhances the likelihood of system convergence by providing greater robustness against uncertainties and disturbances.*
- *Large values of l_3, l_5, l_7 and h_i: These parameters accelerate convergence when the system state exceeds one, ensuring faster stabilization in such scenarios.*
- *Small values of l_4, l_6, l_8: These parameters improve convergence when the system state is less than one, enabling precise control in close proximity to equilibrium.*
- *Small a_i and large r_i: This combination promotes faster convergence when the system state is far from the equilibrium point, ensuring efficient performance in scenarios with significant deviations.*

By adhering to these principles, parameters can be tailored to meet the specific needs of each control system, ensuring optimal performance and robustness.

For all control methods evaluated, the parameters were systematically selected through an iterative process of testing and fine-tuning. This approach involved evaluating the algorithms under identical conditions to optimize their performance in terms of trajectory tracking and robustness.

By fine-tuning the parameters, each method was adjusted to ensure fair and consistent comparison while achieving the best possible control outcomes.

To compare the tracking accuracy of the control methods, the root mean square errors (RMSEs) were calculated after the convergence period (from 2 to 20 s). The results, summarized in Table 2, provide a quantitative assessment of the controllers' performance.

The simulation outcomes are illustrated in Figures 5–10 and detailed in Table 2. The time evolution of the auxiliary system variables is shown in Figure 5. It is evident that these variables can converge to zero rapidly. Figure 6 depicts the trajectory tracking performance of the robot arm's end-effector, while Figure 7 demonstrates the tracking performance at the joint level. From these figures, we can see that all four control methods successfully follow the desired trajectory.

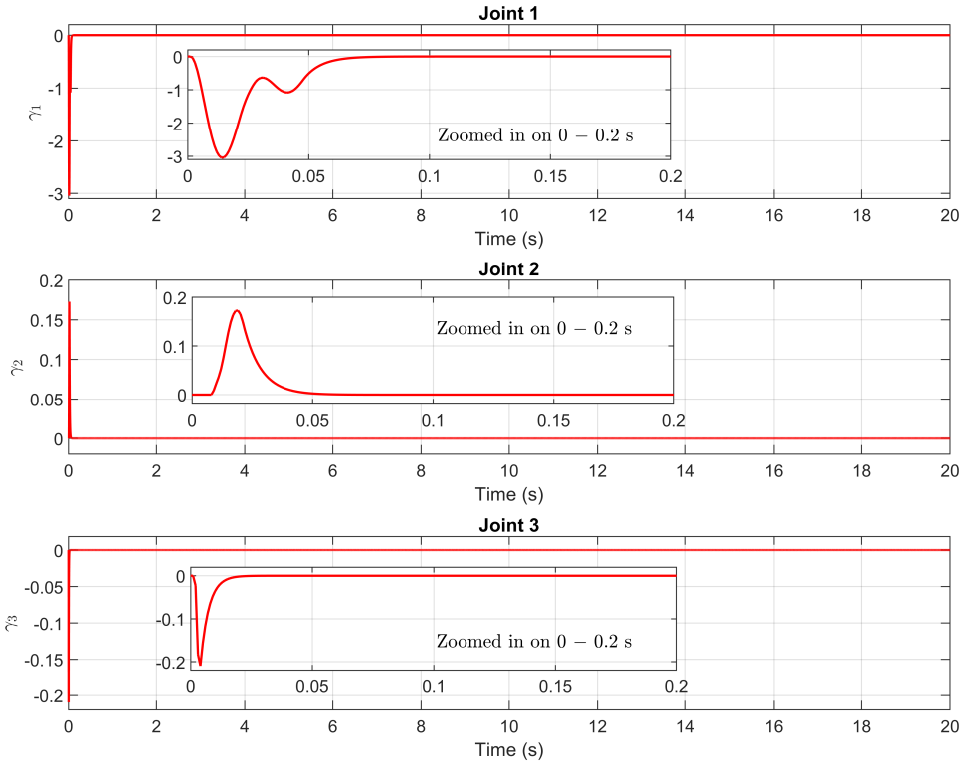

Figure 5. Time evolution of the auxiliary system variables.

The detailed performance comparison is evaluated based on three main criteria: convergence speed, trajectory tracking accuracy and robustness, and chattering suppression in the control signal, providing a comprehensive evaluation of the proposed method's effectiveness.

Convergence speed: Examining the zoomed-in view during the initial period (0 to 0.6 s) in Figure 8, we observe that the NTSMC method exhibits the slowest convergence among the approaches. NFTSMC achieves faster convergence than NTSMC, while GNTSMC further improves the convergence speed compared to NFTSMC. Most notably, the proposed method demonstrates the fastest convergence rate, quickly reaching the steady state. This superior performance is attributed to the new FTSMS and new FTRCL, enabling it to outperform the other three approaches. The convergence time of the proposed method is approximately 0.3 s for all three joints, which is significantly lower than the theoretical maximum settling time ($T_{\max} = 5.21$ s). These results confirm that the proposed method achieves fixed-time convergence under practical conditions, validating the theoretical bounds derived in Theorem 1. Moreover, the consistent convergence time across

joints, even in the presence of estimation errors, uncertainties, and external disturbances, highlights the robustness and reliability of the proposed approach.

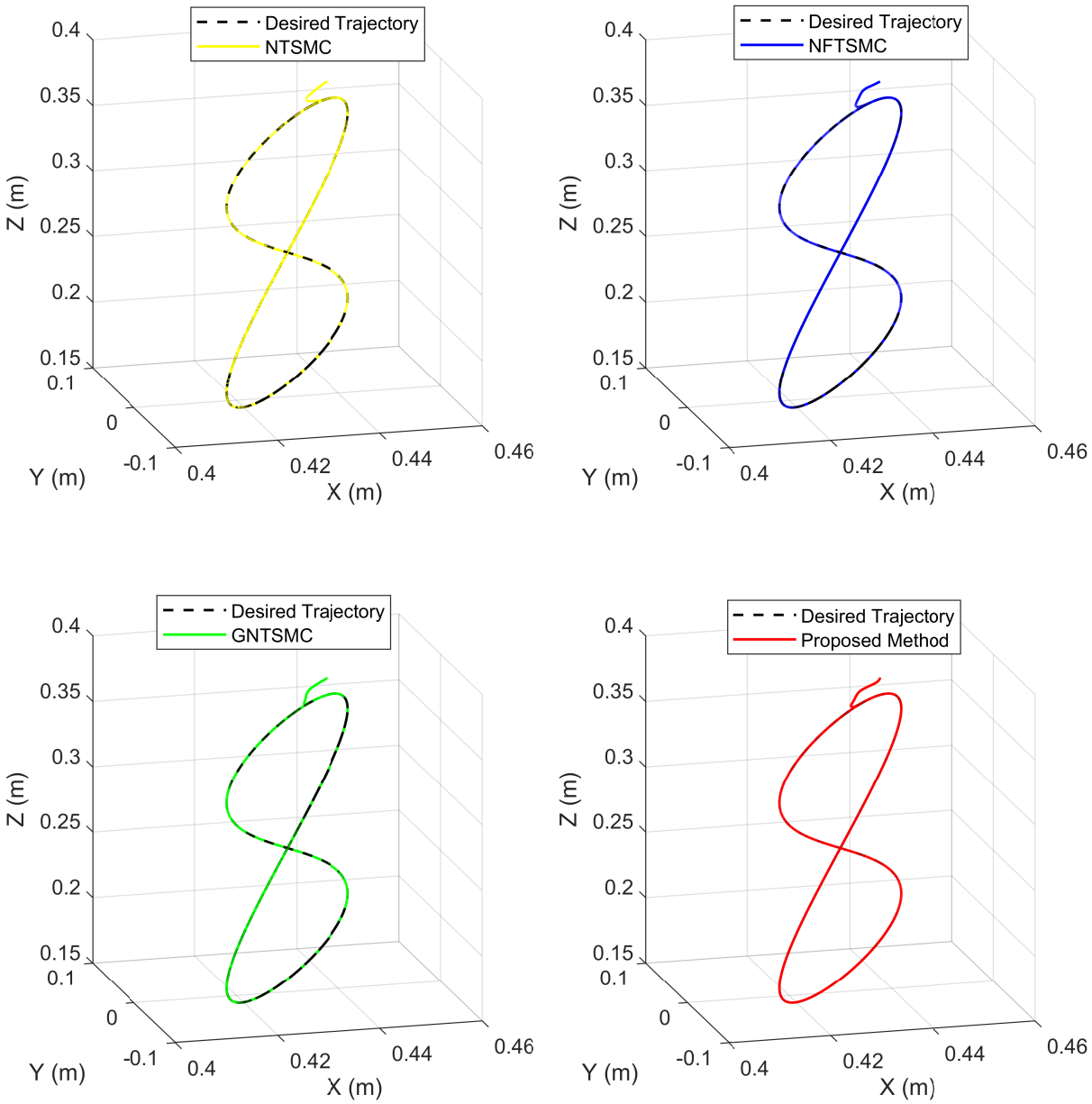

Figure 6. Trajectory tracking performance of the robot end-effector across four control methods.

Trajectory tracking accuracy and robustness: A detailed analysis of the tracking accuracy is provided in Figure 8, which compares the tracking errors at the joints, and Figure 9, which highlights the RMSEs of the control methods. During the period from 0.6 to 20 s, as shown in the zoomed-in view of Figure 8 and the RMSEs in Figure 9, the NTSMC and NFTSMC methods exhibit comparable tracking accuracy. Their tracking errors are within the range of 10^{-4} to 10^{-10} radians, as summarized in Table 2. However, NFTSMC demonstrates slightly superior accuracy compared to NTSMC. The GNTSMC method achieves a further improvement in accuracy, with tracking errors consistently within the range of 10^{-5} radians. Most notably, the proposed method outperforms all others, delivering exceptional tracking precision. Its tracking errors remain consistently within the range of 10^{-7} to 10^{-8} radians, showcasing its significant advantage in ensuring superior accuracy and robustness.

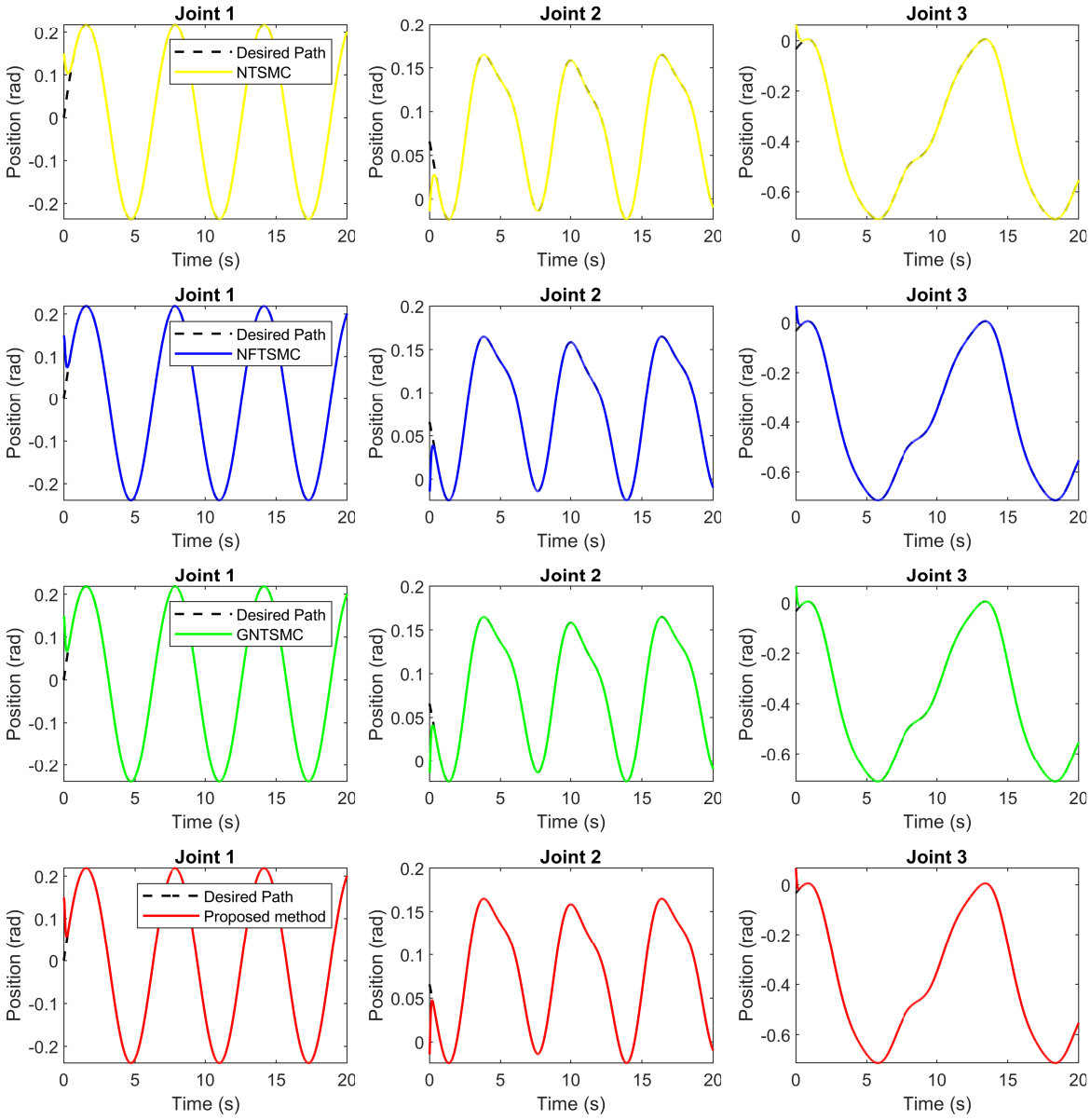

Figure 7. Joint-level trajectory tracking performance across four control methods.

With assumed uncertainties, including uncertain dynamics, friction forces, and external disturbances, the proposed method addresses these issues more effectively than the other methods. Consequently, the tracking accuracy of the proposed method remains consistently high throughout the robot's operation.

Table 2. RMSEs of control methods.

Methods	Joint 1	Joint 2	Joint 3
NTSMC	3.817×10^{-5}	5.737×10^{-5}	2.907×10^{-4}
NFTSMC	3.725×10^{-5}	5.221×10^{-5}	2.435×10^{-4}
GNTSMC	3.306×10^{-5}	2.812×10^{-5}	4.827×10^{-5}
Proposed Method	3.822×10^{-8}	1.065×10^{-7}	9.174×10^{-8}

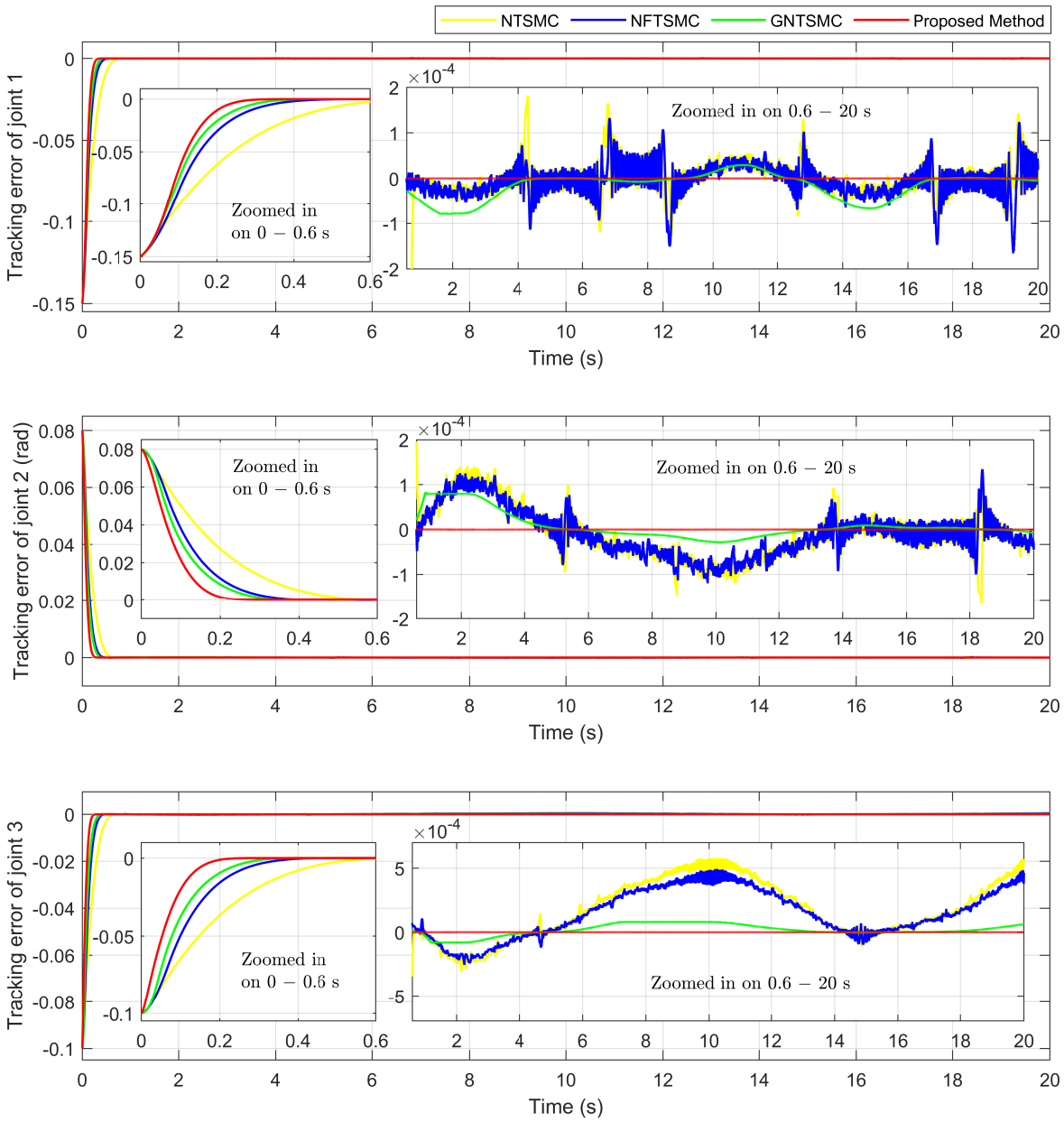

Figure 8. Tracking error comparison under four different control methods.

Chattering suppression: Figure 10 presents a comparison of the control input torques generated by the various methods. It is apparent that both NTSMC and NFTSMC exhibit significant chattering in their control signals. This behavior is attributed to the high sliding gain (κ_1) employed to compensate for the upper bounds of external disturbances and system uncertainties. In contrast, GNTSMC and the proposed method generate substantially smoother control signals, highlighting their enhanced robustness and efficiency. The GNTSMC method leverages a super-twisting algorithm to effectively suppress chattering, while the proposed method achieves similar smoothness with a smaller sliding gain, relying on the TDE approach to handle modeling errors and disturbances. This reduction in gain not only minimizes chattering but also enhances the overall energy efficiency of the control system.

The enlarged views in Figure 10 further reveal instances of actuator saturation at the joints, which could adversely affect system performance. Unlike the other methods, the proposed approach incorporates an auxiliary system to actively compensate for the

effects of input saturation. This feature ensures consistent and reliable tracking performance even under saturation constraints, demonstrating the proposed method's robustness and adaptability in practical applications.

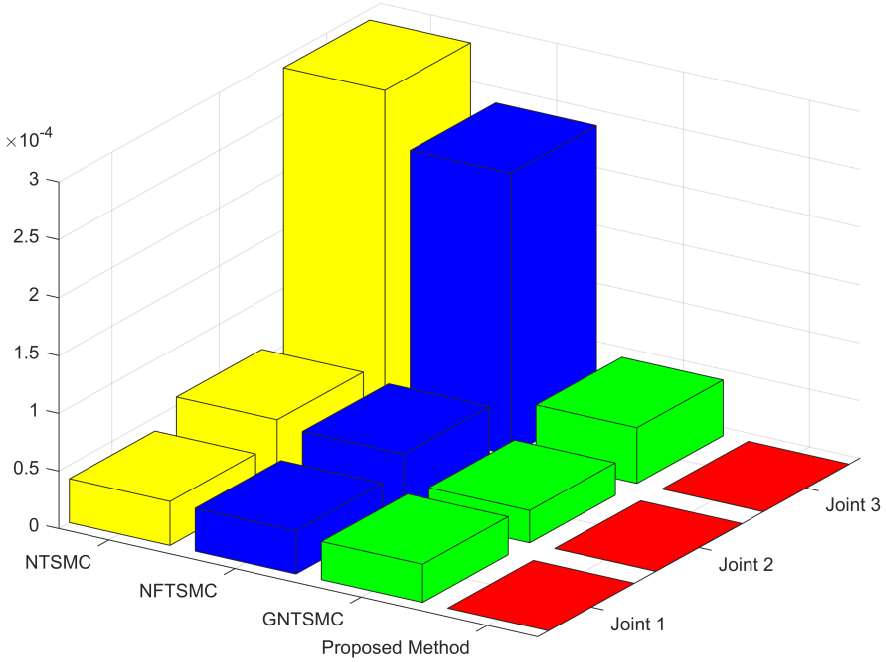

Figure 9. RMSEs across four control methods.

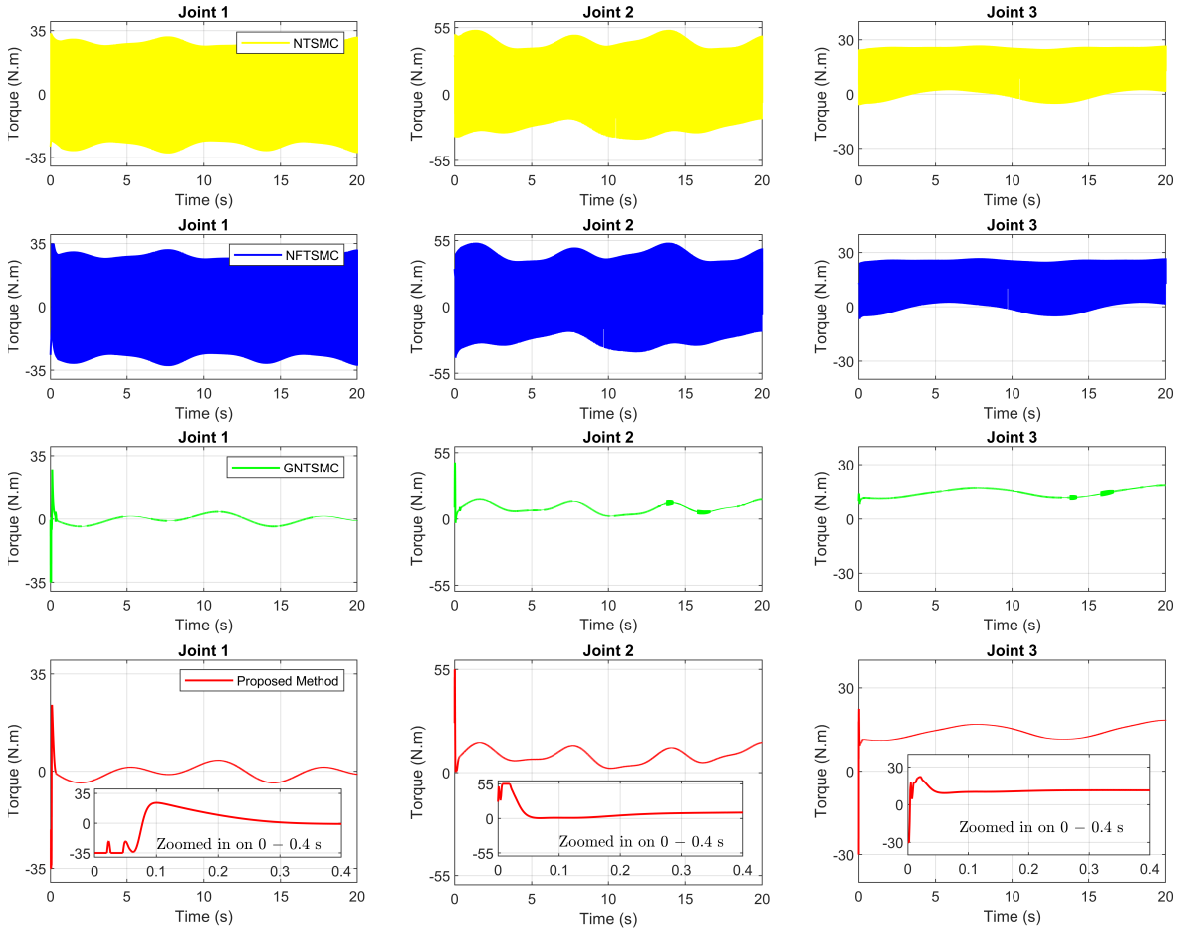

Figure 10. Control input comparison under four different control methods.

Remark 4. *The proposed method introduces additional parameters, which could slightly increase the tuning effort. However, it is important to emphasize that the proposed approach is fundamentally model-free, leveraging the TDE technique to approximate the robot's dynamics without requiring explicit knowledge of its highly nonlinear model. This model-free design offers a significant advantage, particularly for robot manipulators with a large number of DOFs. For such systems, deriving and computing the dynamic model in real-time becomes exceedingly challenging and computationally intensive, often necessitating substantial simplifications or approximations that compromise control performance. By avoiding the need for explicit dynamic modeling, the proposed method simplifies the implementation process and is better suited for high-DOF manipulators operating in dynamic and uncertain environments. Furthermore, the computational overhead introduced by the additional parameters is outweighed by the enhanced robustness, faster convergence, and higher tracking accuracy achieved by the proposed method. These benefits are particularly advantageous in applications requiring precision and reliability under significant uncertainties and disturbances.*

5. Conclusions

This paper proposed an advanced orbit-tracking control approach for robotic manipulators, combining TDE and FSMC techniques to address challenges such as nonlinearities, uncertainties, disturbances, and input saturation. The proposed method integrates a novel NFTSM surface and a novel FTRCL to ensure faster convergence and higher accuracy. An innovative auxiliary system effectively mitigates input saturation effects, maintaining system stability and precision under constraints.

The simulation results on a 3-DOF SAMSUNG FARA AT2 robot manipulator validate the superiority of the proposed approach. It outperforms NTSMC, NFTSMC, and GNTSMC by achieving faster convergence, enhanced tracking accuracy, reduced chattering, and robust performance under uncertainties and disturbances. With its model-free design and fixed-time convergence rigorously proven via Lyapunov theory, the proposed method significantly advances the precision, robustness, and reliability of robotic systems, making it highly suitable for demanding industrial applications requiring high-performance control.

Future work will extend the proposed control approach to nonlinear systems such as UAVs and AUVs, addressing challenges like uncertainties, disturbances, and input saturation. By adapting the NFTSM surface and FTRCL, the method can improve tracking accuracy and robustness while the auxiliary system ensures stability under constraints. Additionally, achieving prescribed performance for these systems is a valuable direction for exploration. Furthermore, a limitation of this paper is the use of a constant matrix in the design of TDE. To address this, future work will incorporate adaptive rules for the matrix, enhancing flexibility and performance under varying system conditions.

Author Contributions: Methodology, conceptualization, writing—original draft preparation, and writing—review, software, and editing, T.N.T.; validation, visualization, resources, and editing A.T.V. and T.N.T.; supervision, funding acquisition, and project administration, H.-J.K.; formal analysis and data curation, A.T.V. and H.-J.K. All authors have read and agreed to the published version of the manuscript.

Funding: This work was funded by University of Ulsan.

Data Availability Statement: Upon reasonable request, the corresponding author can provide the data sets generated and/or analyzed during this study.

Acknowledgments: Our research was supported by University of Ulsan.

Conflicts of Interest: The authors declare no conflicts of interest.

References

1. Alnufaie, L. Nonsingular fast terminal sliding mode controller for a robotic system: A fuzzy approach. *IEEE Access* **2023**, *11*, 75522–75527. [CrossRef]
2. Van, M.; Sun, Y.; Mcllvanna, S.; Nguyen, M.N.; Khyam, M.O.; Ceglarek, D. Adaptive fuzzy fault tolerant control for robot manipulators with fixed-time convergence. *IEEE Trans. Fuzzy Syst.* **2023**, *31*, 3210–3219. [CrossRef]
3. Lee, J.E.; Kim, B.W. Improving Direct Yaw-Moment Control via Neural-Network-Based Non-Singular Fast Terminal Sliding Mode Control for Electric Vehicles. *Sensors* **2024**, *24*, 4079. [CrossRef] [PubMed]
4. Truong, T.N.; Vo, A.T.; Kang, H.J. Neural network-based sliding mode controllers applied to robot manipulators: A review. *Neurocomputing* **2023**, *562*, 126896. [CrossRef]
5. Truong, T.N.; Vo, A.T.; Kang, H.J. A model-free terminal sliding mode control for robots: Achieving fixed-time prescribed performance and convergence. *ISA Trans.* **2024**, *144*, 330–341. [CrossRef] [PubMed]
6. Wang, Y.; Li, S.; Wang, D.; Ju, F.; Chen, B.; Wu, H. Adaptive time-delay control for cable-driven manipulators with enhanced nonsingular fast terminal sliding mode. *IEEE Trans. Ind. Electron.* **2020**, *68*, 2356–2367. [CrossRef]
7. Sun, W.; Wu, Y.; Lv, X. Adaptive neural network control for full-state constrained robotic manipulator with actuator saturation and time-varying delays. *IEEE Trans. Neural Netw. Learn. Syst.* **2021**, *33*, 3331–3342. [CrossRef]
8. Yang, J.; Wang, Y.; Wang, T.; Hu, Z.; Yang, X.; Rodriguez-Andina, J.J. Time-Delay Sliding Mode Control for Trajectory Tracking of Robot Manipulators. *IEEE Trans. Ind. Electron.* **2024**, *71*, 13083–13091. [CrossRef]
9. Lee, J.; Chang, P.H.; Jin, M. Adaptive integral sliding mode control with time-delay estimation for robot manipulators. *IEEE Trans. Ind. Electron.* **2017**, *64*, 6796–6804. [CrossRef]
10. Kim, S.; Bae, J. Force-mode control of rotary series elastic actuators in a lower extremity exoskeleton using model-inverse time delay control. *IEEE/ASME Trans. Mechatronics* **2017**, *22*, 1392–1400. [CrossRef]
11. Zhang, X.; Liu, J.; Gao, Q.; Ju, Z. Adaptive robust decoupling control of multi-arm space robots using time-delay estimation technique. *Nonlinear Dyn.* **2020**, *100*, 2449–2467. [CrossRef]
12. Baek, J.; Cho, S.; Han, S. Practical time-delay control with adaptive gains for trajectory tracking of robot manipulators. *IEEE Trans. Ind. Electron.* **2017**, *65*, 5682–5692. [CrossRef]
13. Park, J.; Kwon, W.; Park, P. An improved adaptive sliding mode control based on time-delay control for robot manipulators. *IEEE Trans. Ind. Electron.* **2022**, *70*, 10363–10373. [CrossRef]
14. Shtessel, Y.; Edwards, C.; Fridman, L.; Levant, A. *Sliding Mode Control and Observation*; Springer: New Yor, NY, USA, 2014; Volume 10.
15. Yu, X.; Feng, Y.; Man, Z. Terminal sliding mode control–an overview. *IEEE Open J. Ind. Electron. Soc.* **2020**, *2*, 36–52. [CrossRef]
16. Shen, X.; Liu, J.; Liu, G.; Zhang, J.; Leon, J.I.; Wu, L.; Franquelo, L.G. Finite-time sliding mode control for NPC converters with enhanced disturbance compensation. *IEEE Trans. Circuits Syst. I Regul. Pap.* **2024** . [CrossRef]
17. Cruz-Ortiz, D.; Chairez, I.; Poznyak, A. Non-singular terminal sliding-mode control for a manipulator robot using a barrier Lyapunov function. *ISA Trans.* **2022**, *121*, 268–283. [CrossRef]
18. Vo, A.T.; Truong, T.N.; Kang, H.J. An Adaptive Prescribed Performance Tracking Motion Control Methodology for Robotic Manipulators with Global Finite-Time Stability. *Sensors* **2022**, *22*, 7834. [CrossRef] [PubMed]
19. Liu, Z.; Zhao, Y.; Zhang, O.; Chen, W.; Wang, J.; Gao, Y.; Liu, J. A novel faster fixed-time adaptive control for robotic systems with input saturation. *IEEE Trans. Ind. Electron.* **2023**, *71*, 5215–5223. [CrossRef]
20. Liu, Z.; Liu, J.; Zhang, O.; Zhao, Y.; Chen, W.; Gao, Y. Adaptive Disturbance Observer-Based Fixed-Time Tracking Control for Uncertain Robotic Systems. *IEEE Trans. Ind. Electron.* **2024**, *71*, 14823–14831. [CrossRef]
21. Truong, T.N.; Vo, A.T.; Kang, H.J. An adaptive terminal sliding mode control scheme via neural network approach for path-following control of uncertain nonlinear systems. *Int. J. Control Autom. Syst.* **2022**, *20*, 2081–2096. [CrossRef]
22. Vo, A.T.; Truong, T.N.; Kang, H.J. Fixed-time rbfnn-based prescribed performance control for robot manipulators: Achieving global convergence and control performance improvement. *Mathematics* **2023**, *11*, 2307. [CrossRef]
23. Vo, A.T.; Truong, T.N.; Kang, H.J.; Le, T.D. A fixed-time sliding mode control for uncertain magnetic levitation systems with prescribed performance and anti-saturation input. *Eng. Appl. Artif. Intell.* **2024**, *133*, 108373. [CrossRef]
24. Truong, T.N.; Vo, A.T.; Kang, H.J. Real-time implementation of the prescribed performance tracking control for magnetic levitation systems. *Sensors* **2022**, *22*, 9132. [CrossRef]
25. Vo, A.T.; Truong, T.N.; Le, Q.D.; Kang, H.J. Fixed-time sliding mode-based active disturbance rejection tracking control method for robot manipulators. *Machines* **2023**, *11*, 140. [CrossRef]
26. Zou, H.; Zhang, G.; Hao, J. Nonsingular fast terminal sliding mode tracking control for underwater glider with actuator physical constraints. *ISA Trans.* **2024**, *146*, 249–262. [CrossRef]
27. Zhang, L.; Su, Y.; Wang, Z.; Wang, H. Fixed-time terminal sliding mode control for uncertain robot manipulators. *ISA Trans.* **2024**, *144*, 364–373. [CrossRef] [PubMed]
28. Levant, A. Chattering analysis. *IEEE Trans. Autom. Control* **2010**, *55*, 1380–1389. [CrossRef]

29. Hu, J.; Zhang, D.; Wu, Z.G.; Li, H. Neural network-based adaptive second-order sliding mode control for uncertain manipulator systems with input saturation. *ISA Trans.* **2023**, *136*, 126–138. [CrossRef] [PubMed]
30. Santibañez, V.; Camarillo, K.; Moreno-Valenzuela, J.; Campa, R. A practical PID regulator with bounded torques for robot manipulators. *Int. J. Control Autom. Syst.* **2010**, *8*, 544–555. [CrossRef]
31. Huang, J.; Wen, C.; Wang, W.; Jiang, Z.P. Adaptive stabilization and tracking control of a nonholonomic mobile robot with input saturation and disturbance. *Syst. Control Lett.* **2013**, *62*, 234–241. [CrossRef]
32. Sebastian, G.; Tan, Y.; Oetomo, D. Convergence analysis of feedback-based iterative learning control with input saturation. *Automatica* **2019**, *101*, 44–52. [CrossRef]
33. Ma, Z.; Huang, P. Adaptive neural-network controller for an uncertain rigid manipulator with input saturation and full-order state constraint. *IEEE Trans. Cybern.* **2020**, *52*, 2907–2915. [CrossRef]
34. Gao, Y.F.; Sun, X.M.; Wen, C.; Wang, W. Adaptive tracking control for a class of stochastic uncertain nonlinear systems with input saturation. *IEEE Trans. Autom. Control* **2016**, *62*, 2498–2504. [CrossRef]
35. Tong, S.; Li, Y. Adaptive fuzzy output feedback tracking backstepping control of strict-feedback nonlinear systems with unknown dead zones. *IEEE Trans. Fuzzy Syst.* **2011**, *20*, 168–180. [CrossRef]
36. Guo, X.G.; Wang, J.L.; Liao, F.; Teo, R.S.H. CNN-based distributed adaptive control for vehicle-following platoon with input saturation. *IEEE Trans. Intell. Transp. Syst.* **2017**, *19*, 3121–3132. [CrossRef]
37. Zuo, Z. Non-singular fixed-time terminal sliding mode control of non-linear systems. *IET Control Theory Appl.* **2015**, *9*, 545–552. [CrossRef]
38. Yu, L.; He, G.; Wang, X.; Zhao, S. Robust Fixed-Time Sliding Mode Attitude Control of Tilt Trirotor UAV in Helicopter Mode. *IEEE Trans. Ind. Electron.* **2022**, *69*, 10322–10332. [CrossRef]
39. Zhang, L.; Wang, Y.; Hou, Y.; Li, H. Fixed-time sliding mode control for uncertain robot manipulators. *IEEE Access* **2019**, *7*, 149750–149763. [CrossRef]
40. Jin, M.; Lee, J.; Chang, P.H.; Choi, C. Practical nonsingular terminal sliding-mode control of robot manipulators for high-accuracy tracking control. *IEEE Trans. Ind. Electron.* **2009**, *56*, 3593–3601.
41. Jin, M.; Kang, S.H.; Chang, P.H.; Lee, J. Robust Control of Robot Manipulators Using Inclusive and Enhanced Time Delay Control. *IEEE/ASME Trans. Mechatronics* **2017**, *22*, 2141–2152. [CrossRef]
42. Baek, J.; Kwon, W.; Kim, B.; Han, S. A Widely Adaptive Time-Delayed Control and Its Application to Robot Manipulators. *IEEE Trans. Ind. Electron.* **2019**, *66*, 5332–5342. [CrossRef]
43. Yuan, S.-s.; Deng, W.-x.; Yao, J.-y.; Yang, G.-l. Robust control for bidirectional stabilization system with time delay estimation. *Int. J. Control Autom. Syst.* **2024**, *22*, 1163–1175. [CrossRef]
44. Wang, L.; Chai, T.; Zhai, L. Neural-network-based terminal sliding-mode control of robotic manipulators including actuator dynamics. *IEEE Trans. Ind. Electron.* **2009**, *56*, 3296–3304. [CrossRef]
45. Zhai, J.; Xu, G. A Novel Non-Singular Terminal Sliding Mode Trajectory Tracking Control for Robotic Manipulators. *IEEE Trans. Circuits Syst. II Express Briefs* **2021**, *68*, 391–395. [CrossRef]
46. Yang, L.; Yang, J. Nonsingular fast terminal sliding-mode control for nonlinear dynamical systems. *Int. J. Robust Nonlinear Control* **2011**, *21*, 1865–1879. [CrossRef]
47. Sun, C.; Huang, Z.; Wu, H. Adaptive super-twisting global nonsingular terminal sliding mode control for robotic manipulators. *Nonlinear Dyn.* **2024**, *112*, 5379–5389. [CrossRef]